nature medicine

ARTICLES

https://doi.org/10.1038/s41591-020-1043-9



# Neuronal defects in a human cellular model of 22q11.2 deletion syndrome

Themasap A. Khan[1,2,20], Omer Revah[1,20], Aaron Gordon[3,20], Se-Jin Yoon[1], Anna K. Krawisz[4,18], Carleton Goold[4], Yishan Sun[4], Chul Hoon Kim[4,5], Yuan Tian[3,6], Min-Yin Li[1], Julia M. Schaepe[1], Kazuya Ikeda[7], Neal D. Amin[1], Noriaki Sakai[1], Masayuki Yazawa[4,19], Leila Kushan[8], Seiji Nishino[1], Matthew H. Porteus[7], Judith L. Rapoport[9], Jonathan A. Bernstein[7], Ruth O'Hara[1], Carrie E. Bearden[8,10,11], Joachim F. Hallmayer[1], John R. Huguenard[12], Daniel H. Geschwind[3,13,14,15], Ricardo E. Dolmetsch[16] and Sergiu P. Pașca[1,17] ✉

**22q11.2 deletion syndrome (22q11DS) is a highly penetrant and common genetic cause of neuropsychiatric disease. Here we generated induced pluripotent stem cells from 15 individuals with 22q11DS and 15 control individuals and differentiated them into three-dimensional (3D) cerebral cortical organoids. Transcriptional profiling across 100 days showed high reliability of differentiation and revealed changes in neuronal excitability-related genes. Using electrophysiology and live imaging, we identified defects in spontaneous neuronal activity and calcium signaling in both organoid- and 2D-derived cortical neurons. The calcium deficit was related to resting membrane potential changes that led to abnormal inactivation of voltage-gated calcium channels. Heterozygous loss of *DGCR8* recapitulated the excitability and calcium phenotypes and its overexpression rescued these defects. Moreover, the 22q11DS calcium abnormality could also be restored by application of antipsychotics. Taken together, our study illustrates how stem cell derived models can be used to uncover and rescue cellular phenotypes associated with genetic forms of neuropsychiatric disease.**

A central challenge in studying the pathophysiological mechanisms leading to neurodevelopmental disorders, such as schizophrenia (SCZ) or autism spectrum disorder (ASD), is the heterogeneity of these behaviorally defined conditions[1]. One approach to overcome this complexity is to study patients with highly penetrant genetic mutations[2]. The 22q11.2 deletion syndrome (22q11DS) is the most frequent (1:3,000) genetic deletion in humans[3]. Up to one in four 22q11DS patients develop psychosis, which corresponds to an ~20-fold increase in risk and accounts for 1–2% of all SCZ cases[4–6]. This microdeletion also confers a 30–40% risk for ASD[7,8]. This genetic syndrome provides an opportunity to begin addressing the heterogeneity of neuropsychiatric disorders and to identify neuronal phenotypes.

Rodent models of 22q11DS have provided important insights[3,9,10], including describing circuit dysfunction[11–13]. However, human neuronal phenotypes, especially in the context of the unique genomic structure of the human 22q11.2 locus[14], remain poorly understood. Therefore, novel approaches to capture the pathobiology of this genetic deletion are required. Cellular reprogramming technologies allow the in vitro generation of human neurons[15]. These models maintain the genetic background of the individuals from which the human induced pluripotent stem (hiPS) cells were derived. Recent studies[16–18] have begun to explore transcriptional changes in neural cells derived from a small 22q11DS cohort, but the functional defects in human 22q11DS neurons and the underlying mechanisms have not been investigated.

To better understand the neuronal pathways leading to disease in 22q11DS, we differentiated 43 hiPS cell lines derived from 15 individuals carrying the canonical 3-Mb 22q11.2 deletion and 15 control subjects. We derived three-dimensional (3D) human cortical spheroids (hCSs)[19–21], which are regionalized brain organoids that show high reliability of differentiation[22], as well as cortical glutamatergic cultures using 2D differentiation[23,24]. Transcriptional analyses performed over 100 days of 3D differentiation indicated

[1]Department of Psychiatry and Behavioral Sciences, Stanford University, Stanford, CA, USA. [2]Program in Stem Cell Biology and Regenerative Medicine, Stanford University, Stanford, CA, USA. [3]Program in Neurogenetics, Department of Neurology, University of California Los Angeles, Los Angeles, CA, USA. [4]Department of Neurobiology, Stanford University, Stanford, CA, USA. [5]Department of Pharmacology, Yonsei University College of Medicine, Seoul, Republic of Korea. [6]Interdepartmental PhD Program in Bioinformatics, University of California Los Angeles, Los Angeles, CA, USA. [7]Department of Pediatrics, Stanford University, Stanford, CA, USA. [8]Department of Psychiatry and Biobehavioral Sciences, University of California Los Angeles, Los Angeles, CA, USA. [9]National Institute of Mental Health, Child Psychiatry Branch, Bethesda, MD, USA. [10]Department of Psychology, University of California Los Angeles, Los Angeles, CA, USA. [11]Center for Neurobehavioral Genetics, Semel Institute for Neuroscience and Human Behavior, University of California Los Angeles, Los Angeles, CA, USA. [12]Department of Neurology and Neurological Sciences, Stanford University, Stanford, CA, USA. [13]Department of Human Genetics, David Geffen School of Medicine, University of California Los Angeles, Los Angeles, CA, USA. [14]Center for Autism Research and Treatment, Semel Institute, University of California Los Angeles, Los Angeles, CA, USA. [15]Institute of Precision Health, University of California Los Angeles, Los Angeles, CA, USA. [16]Novartis Institutes for BioMedical Research, Cambridge, MA, USA. [17]Stanford Brain Organogenesis Program, Wu Tsai Neurosciences Institute, Stanford University, Stanford, CA, USA. [18]Present address: Division of Cardiology, Department of Medicine, Beth Israel Deaconess Medical Center, Boston, MA, USA. [19]Present address: Columbia Stem Cell Initiative, Department of Rehabilitation and Regenerative Medicine, Department of Molecular Pharmacology and Therapeutics, Vagelos College of Physicians and Surgeons, Columbia University, New York, NY, USA. [20]These authors contributed equally: Themasap A. Khan, Omer Revah, Aaron Gordon. ✉e-mail: spasca@stanford.edu

abnormal neuronal excitability. We found changes in spontaneous firing and depolarization-induced calcium signaling in 22q11DS cortical neurons. This was related to abnormalities in the resting membrane potential (RMP), which led to defects in the function of the disease-associated[25,26] voltage gated L-type calcium channels (LTCC). Moreover, the calcium and membrane potential alterations were phenocopied in an isogenic hiPS cell line carrying a mutation in the 22q11.2 locus gene *DGCR8* and were restored by viral delivery of this transcript. Finally, these defects were rescued by short exposure to antipsychotics, which are known to influence excitability and LTCC[27]. Taken together, these experiments identify key cellular phenotypes for 22q11DS in human neurons and have the potential for identifying therapeutic approaches.

## Results

**Cortical differentiation and transcriptomic changes in 22q11DS.** We used cell reprogramming to generate hiPS cells from fibroblasts taken from a cohort of 15 patients with 22q11DS (22.8 ± 2.4 years; female to male, 60% to 40%) and 15 controls (23.8 ± 4.0 years; female to male, 67% to 33%; Supplementary Tables 1–3 and Extended Data Fig. 1a,b). We used single nucleotide polymorphism (SNP) arrays to verify genome integrity and to confirm the 22q11.2 deletion (Extended Data Fig. 1c and Supplementary Table 4). Next, we differentiated 43 hiPS cell lines using a directed differentiation approach to derive hCSs (Fig. 1a)[19–21]. hCSs transcriptionally resemble the developing cerebral cortex, contain functional glutamatergic neurons and astrocytes, and their generation is highly reliable across differentiation experiments and lines[22].

To analyze the transcriptomic changes during corticogenesis, we collected RNA at days 25, 50, 75 and 100 from 15 hiPS cell lines derived from 12 22q11DS individuals in 17 differentiation experiments and 14 hiPS cell lines from 11 controls in 26 differentiation experiments (Extended Data Fig. 2a).

We first established the reproducibility of differentiation[22]. We found high Spearman's correlation coefficients (mean ≈ 0.97) between differentiations of the same cell line (within individuals) and between different hiPS cell lines ($P < 0.05$; Extended Data Fig. 2b,c), for matched differentiation days. We next used principal component analysis (PCA) to interrogate the transcriptional variance between differentiations (Fig. 1b,c). The main source of variation was related to the stage of differentiation, with the first principal component (PC1) explaining 33% of the variance, similar to what we observed previously[22]. Genetic ancestry explained a small portion of the variance (Extended Data Fig. 2d). PC2 (7.4%), as well as PC5, PC6 and PC7 (8.1% combined), were related to differences between the 22q11DS and control groups. Furthermore, variance partitioning showed that differentiation time explained 28% of the variance on average, while the differentiation experiment and the hiPS cell line explained 9.3% and 3.9% of the variance, respectively (Extended Data Fig. 2e). We next performed single-cell transcriptomics in four different hiPS cell lines (Extended Data Fig. 3a,b). Clustering of cells using *t*-distributed stochastic neighbor embedding (*t*-SNE) revealed a separation of *STMN2*-expressing neurons from progenitors and mitotically active cells expressing *VIM* and *TOP2A* (Extended Data Fig. 3c). We also identified a group of glutamatergic neurons (*VGLUT1*$^+$) expressing the cortical layer markers *TBR1*; a group of intermediate progenitors expressing *EOMES*; a group of dorsal progenitors expressing *PAX6*; a group of astroglia (*CLU*$^+$); a small group of cells that resemble the choroid plexus (*TTR*$^+$, *SLC13A4*$^+$) and a very small number of *GAD1*$^+$ cells. We then compared expression of all detected genes across all four lines and we found that they were highly correlated (Extended Data Fig. 3d,g). Similarly, we found that gene expression in each domain was highly correlated across lines (Extended Data Fig. 3e). We also compared the proportion of cells in each cluster across lines and found that cell diversity was overall similar across lines and groups (Extended Data Fig. 3f). Finally, to investigate potential disease-related differences in differentiation, we verified the temporal trajectories of gene expression for selected cortical markers and found high consistency (Extended Data Fig. 4a). Together, these data demonstrate the high reliability of hCSs, suggesting that defects in early cortical differentiation may not be substantial contributors to developmental defects in 22q11DS.

We next examined gene expression patterns within the 22q11.2 locus by bulk RNA-seq (Fig. 1d). We found that 57 genes were expressed in hCSs, which overlapped with the 67 genes from this chromosomal region shown to be expressed in human fetal brain tissue (Extended Data Fig. 2f)[28]. The majority of protein-coding genes were downregulated in 22q11DS hCS by ~50% (Extended Data Fig. 2g), except for *DGCR8*, which was downregulated by ~20%. We then performed differential expression analysis in hCSs derived from 29 hiPS cell lines to investigate the genome-wide effects of the microdeletion. A power analysis based on our first batch indicated an 85% power of detecting ~18% change in expression (Extended Data Fig. 2h). We identified 87, 34, 258 and 46 differentially expressed genes (DEGs, FDR < 0.05) at days 25, 50, 75 and 100, respectively (Fig. 1e and Supplementary Table 5). DEGs were broadly expressed across cell types (Extended Data Fig. 3h). A DEG subset overlapped with transcriptomic changes in a 22q11DS human model[18], but we found no overlap with a mouse model[29] (Extended Data Fig. 2i). Using gene set enrichment analysis (GSEA) we found changes in genes associated with RNA modification and gene silencing by RNA that may be related to loss of *DGCR8*[30] (Fig. 1f and Supplementary Table 6). We also found enrichment for genes related to mitochondrial function[31] (Extended Data Fig. 4b). Moreover, we observed an enrichment for genes related to neuronal excitability, including genes related to regulation of calcium transport, calcium signaling, RMP or voltage-gated calcium channel activity. Finally, to test whether DEGs in 22q11DS were enriched for psychiatric disease genes, we verified enrichment of SNP heritability in genome-wide association studies (GWAS) for ASD[32], SCZ[33] and ADHD[34] (Fig. 1g). We observed an enrichment for variants associated with SCZ, but not for DEG found in ASD or SCZ postmortem brain tissue[35,36].

**Defects in cortical neuronal excitability and calcium signaling in 22q11DS.** The changes in excitability genes prompted us to investigate the intrinsic electrophysiological properties of cortical neurons. We performed cell-attached and whole-cell patch-clamp recordings in dissociated hCS neurons at 70–80 days (Extended Data Fig. 5a) that were labeled with adeno-associated virus (AAV)–Syn1::YFP. We found that 22q11DS cells were approximately four times more likely to spontaneously fire action potentials (APs) than controls ($P = 0.001$; Fig. 2a,b; $P = 0.0006$; Extended Data Fig. 5b). We next tested whether the increased spontaneous firing in 22q11DS is associated with intrinsic changes in AP firing (Fig. 2c). In neurons that fired at least one AP (93% in 22q11DS and 74% in controls), we found no differences in AP amplitude ($P = 0.69$), threshold ($P = 0.97$), rheobase ($P = 0.22$), maximal rate of rise ($P = 0.29$) and maximal rate of decay ($P = 0.43$) between 22q11DS and control neurons (Extended Data Fig. 5c). This suggests that the ability to generate APs is not affected in 22q11DS cortical neurons.

We next investigated whether the abnormal neuronal excitability in 22q11DS neurons is coupled with changes in calcium signaling during depolarization. We examined intracellular calcium levels ($[Ca^{2+}]_i$) in dissociated, Syn1$^+$ hCS neurons using the ratiometric calcium indicator Fura-2 and time-lapse microscopy. In 22q11DS neurons we observed a decrease in the amplitude of $[Ca^{2+}]_i$ rise following 67 mM KCl depolarization (Fig. 2d); this was consistent across the cohort (Fig. 2e, left; $P < 0.0001$). A mixed-model analysis of variance (ANOVA) indicated that variability across lines explained only 19.9% of the variance in the phenotype (Fig. 2e, right; $P < 0.0001$). We did not observe differences in $[Ca^{2+}]_i$ between

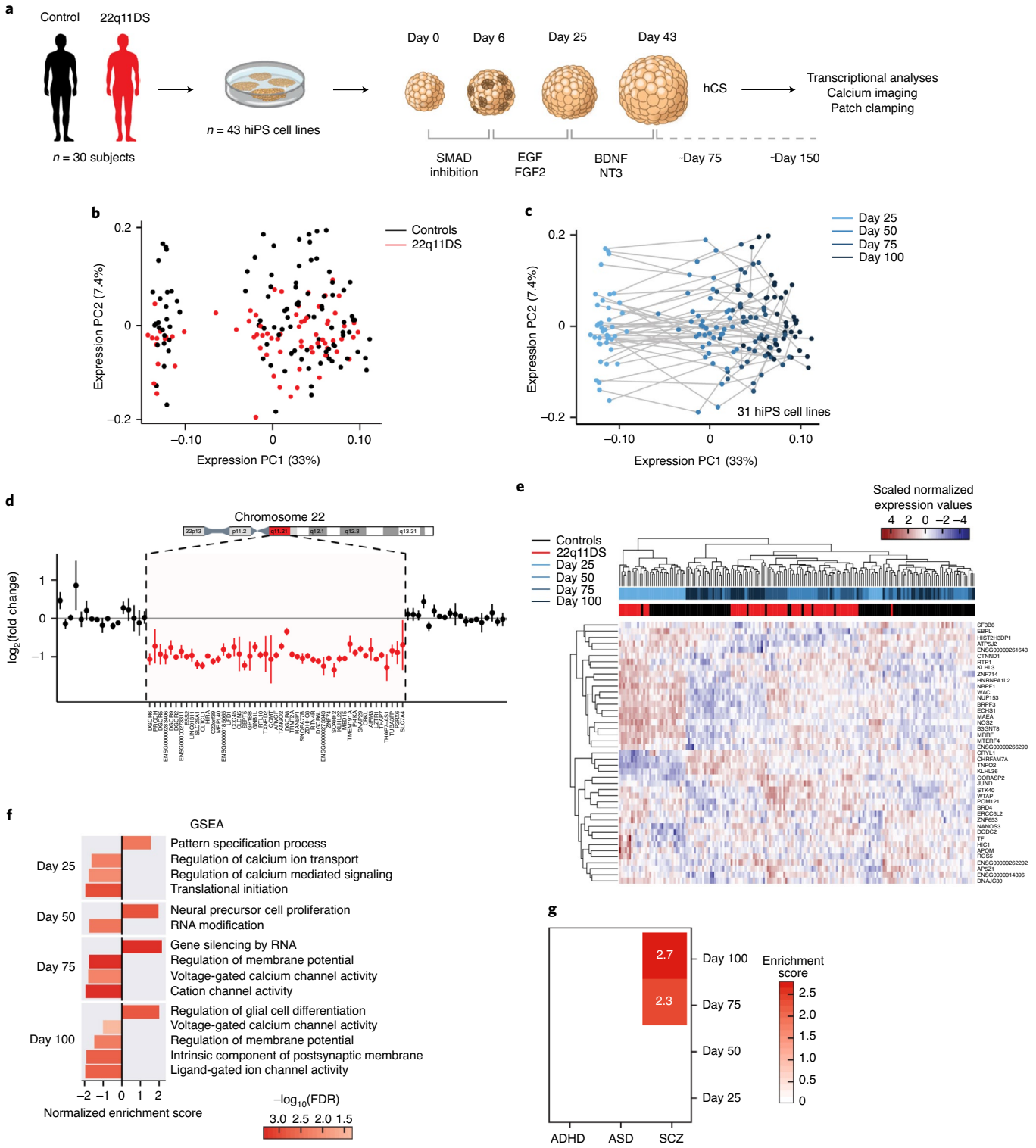


**Fig. 1 | Cortical differentiation and transcriptomic changes in 22q11DS. a**, Scheme illustrating the generation and analysis of hCSs from control and 22q11DS (23 hiPS cell lines from 15 controls and 20 hiPS cell lines from 15 22q11DS). **b**,**c**, PCA of gene expression over time in vitro. In **b**, PC2 (7.4%) is associated with the presence of the 22q11.2 deletion. In **c**, PC1 (33%) is associated with differentiation time (shades of blue) and each differentiation is delineated by a gray line. **d**, The 57 genes in the 22q11.2 locus (highlighted area) are downregulated across 22q11DS. Points represent $\log_2$(fold change) of the gene and bars represent 95% confidence intervals. **e**, Heatmap of expression of the top differentially expressed gene (DEG) based on hierarchical clustering (87, 34, 258 and 46 DEGs at false discovery rate (FDR) < 0.05 at days 25, 50, 75 and 100, respectively). **f**, Select terms from gene set enrichment analysis (GSEA). The scale indicates FDR. **g**, Enrichment for the genome-wide association study (GWAS) signal from ASD, ADHD and SCZ. Numbers and colors represent the enrichment score (FDR < 0.05). In **b**–**g**, control: $n = 104$ samples from 14 control hiPS cell lines derived from 11 subjects; 22q11DS: $n = 71$ samples derived from 15 patient hiPS cell lines derived from 12 subjects.

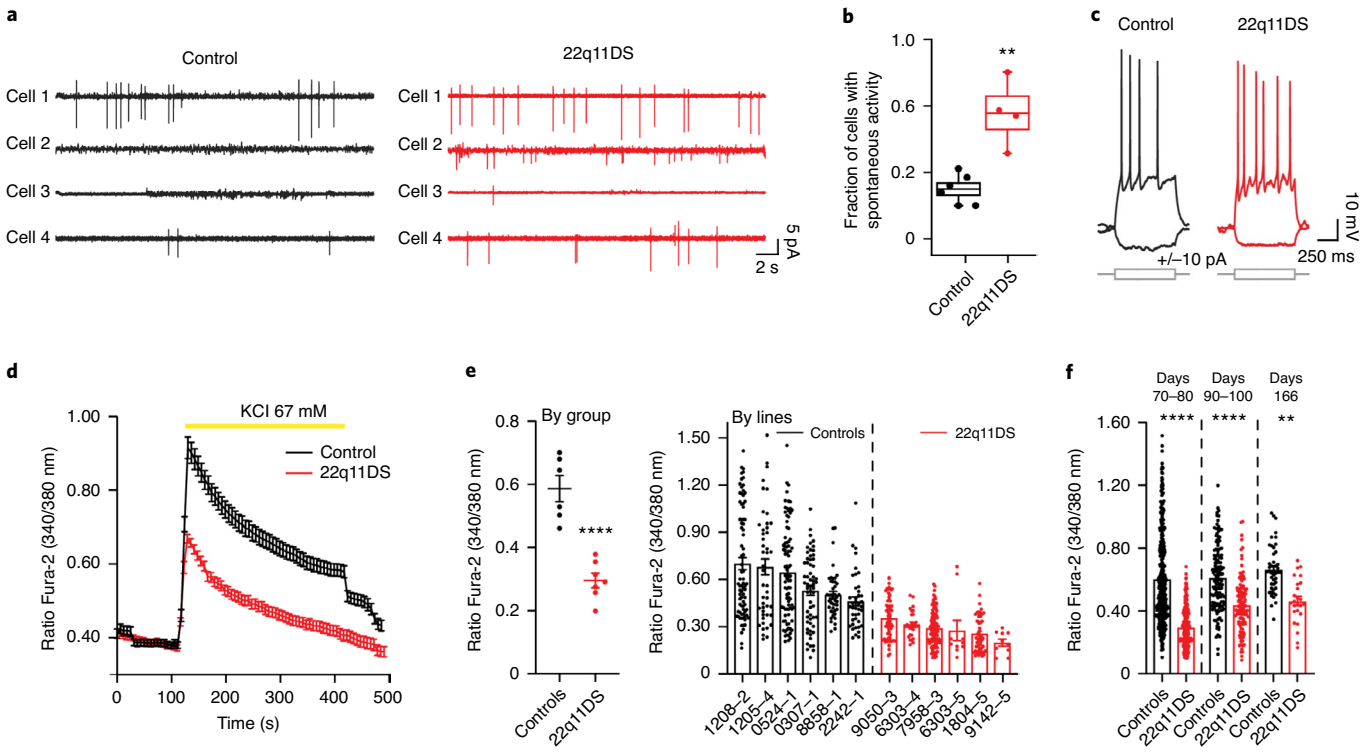


**Fig. 2 | Defects in neuronal excitability and calcium signaling in 22q11DS neurons. a**, Representative traces from dissociated hCS neurons showing spontaneous APs recorded in cell-attached mode from control and 22q11DS neurons (control, $n=4$ cells from four hiPS cell lines derived from four subjects; 22q11DS, $n=4$ cells from four hiPS cell lines derived from three subjects). **b**, Proportion of cells with spontaneous APs from dissociated hCS neurons (controls, $n=44$ cells derived from six control hiPS cell lines derived from six subjects; 22q11DS, $n=60$ cells derived from four patient hiPS cell lines derived from three subjects; chi-squared test, $\chi^2=11.52$, $^{***}P=0.0006$). The center line shows the median, the box shows s.e.m. and the whiskers represent the 10th and 90th percentiles. **c**, Representative traces from dissociated hCS neurons, showing repetitive AP firing in response to current injection. **d**, Changes in Fura-2 ratio in response to 67 mM KCl in dissociated hCS neurons (control, $n=119$ cells derived from three hiPS cell lines and three subjects; 22q11DS, $n=108$ cells derived from three hiPS cell lines and three subjects). Traces are from a representative experiment (the complete quantified dataset is shown in **e**). Data are presented as mean ratio ± s.e.m. **e**, Quantification of $[Ca^{2+}]_i$ amplitude shown (left) per group (two-tailed $t$-test, $^{****}P<0.0001$) and (right) per hiPS cell line ($n=6$ 22q11DS lines, $n=6$ control lines, ANOVA mixed-model analysis $P<0.0001$). Data are presented as mean peak amplitude ± s.e.m. **f**, Quantification of Fura-2 ratio amplitudes over hCS maturation in dissociated hCS neurons (controls: day 70–80, $n=360$ cells from six hiPS cell lines derived from six subjects; day 90–100, $n=136$ cells from three hiPS cell lines derived from three subjects; day 166, $n=46$ cells from two hiPS cell lines derived from two subjects; 22q11DS: day 70–80, $n=365$ cells from six hiPS cell lines derived from five subjects; day 90–100, $n=112$ cells from two hiPS cell lines derived from two subjects, day 166, $n=25$ cells from two hiPS cell lines derived from two subjects). Two-way ANOVA for timepoints, $F_{2,951}=15.75$, $^{****}P<0.0001$; Tukey's multiple comparison test, $^{****}P<0.0001$ for days 70–80, $^{****}P<0.0001$ for days 80–90, $^{**}P=0.003$ for day 166). Data are presented as mean peak amplitude ± s.e.m.

individuals with versus individuals without psychosis ($P=0.88$), although the proportion of our cohort with ascertained psychiatric diagnoses was limited. We also tested if this defect is present in 22q11DS neurons derived with a different 2D cortical differentiation method[23,37] (Extended Data Fig. 6a,b). We similarly found a decrease in the amplitude of $[Ca^{2+}]_i$ rise following depolarization (Extended Data Fig. 6c; $P<0.0001$). A mixed model indicated that variability across lines explained only 2.6% of the variance (Extended Data Fig. 6d, right; $P<0.0003$). Taken together, these experiments in 2D and 3D cortical neurons indicate that this phenotype was robust and consistent across 10 22q11DS lines as compared to 10 control subjects (Cohen's $d=3.76$ for hCSs and 4.37 for 2D neurons).

We next asked whether the calcium changes were present over time during in vitro maturation. We found that although there was an ~48% increase in the amplitude of the $[Ca^{2+}]_i$ rise in 22q11DS neurons from days 70–80 to days 90–100, the overall defect was present even after 5.5 months of differentiation (Fig. 2f; $P<0.0001$; $P<0.0001$ for days 70–80, $P<0.0001$ for days 80–90, $P=0.003$ for day 166).

In exploring the depolarization-induced calcium rise, we found that pretreatment with nimodipine, a blocker of LTCCs, decreased the amplitude of the $[Ca^{2+}]_i$ rise by ~64% in control cortical and by ~57% in 22q11DS (Extended Data Fig. 7a,b; $P<0.0001$). To test the contribution of voltage-gated sodium channels, we used the sodium channel blocker tetrodotoxin (TTX). We found a decrease in the amplitude of the $[Ca^{2+}]_i$ rise, but the difference between 22q11DS and control was still present following TTX (Extended Data Fig. 7c,d; $P=0.03$). To verify the contribution of *N*-methyl-D-aspartate (NMDA) and α-amino-3-hydroxy-5-methyl-4-isoxazolepropionic acid (AMPA) receptors, we applied the 2,3-dioxo-6-nitro-7-sulfamoyl-benzo[f]quinoxaline (NBQX) and (2R)-amino-5-phosphonovaleric acid; (2R)-amino-5-phosphonopentanoate (APV) blockers, and found little or no effect on the $[Ca^{2+}]_i$ rise amplitude following exposure and between groups (Extended Data Fig. 7e,f; $P=0.77$).

To test whether the $[Ca^{2+}]_i$ defect was cell non-autonomous, for example due to a difference in neurotransmitter released during depolarization, we measured the level of catecholamines, glutamate (GLUT) and gamma-aminobutyric acid (GABA), by high-performance liquid chromatography (HPLC). We found either undetectable levels (dopamine (DA), GABA) or no change (GLUT, norepinephrine (NE)) between groups (Extended Data Fig. 8a–d). We also co-cultured

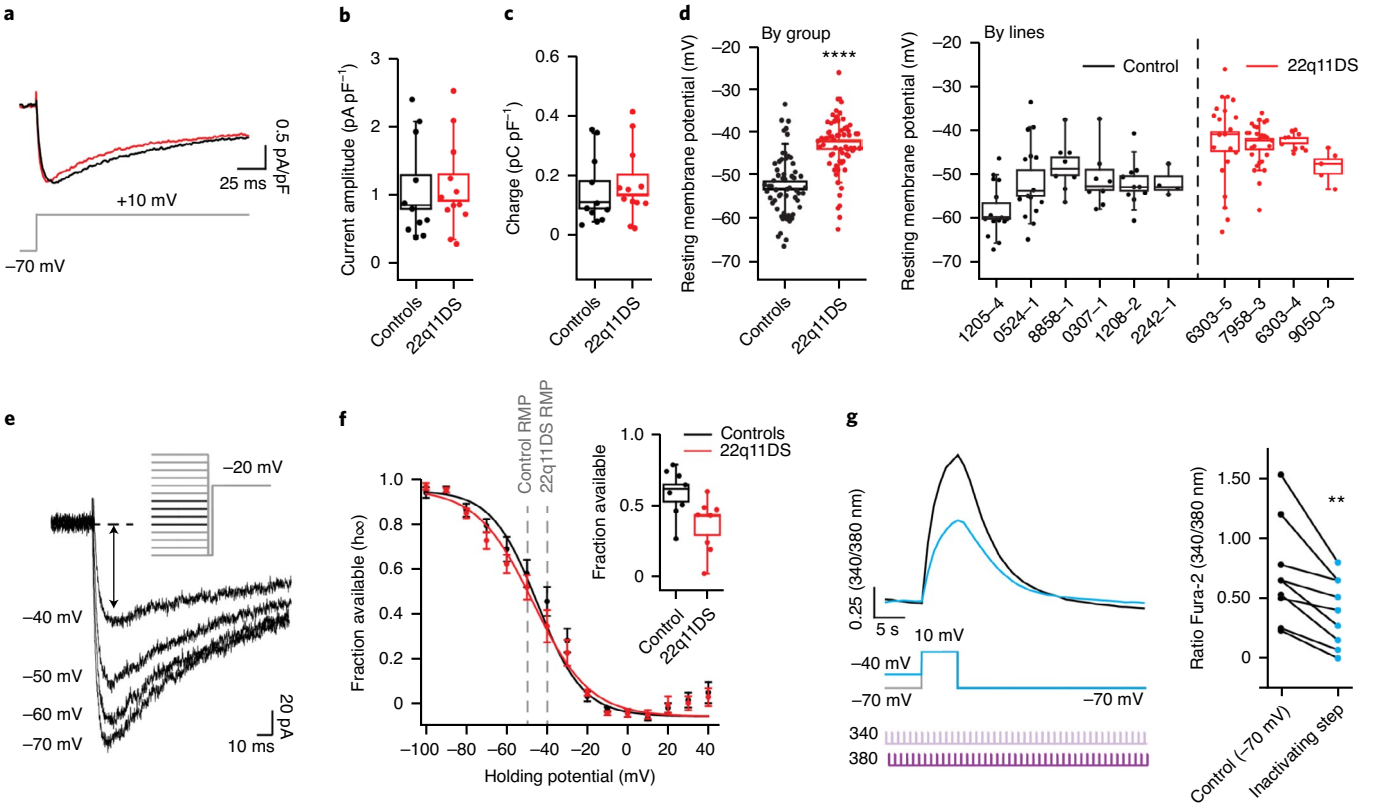


**Fig. 3 | Calcium channel function and RMP in 22q11DS neurons a**, Barium currents in response to a depolarizing step to +10mV. **b**, Barium current amplitude and charge (control, *n*=11 cells from two hiPS cell lines derived from two subjects; 22q11DS, *n*=12 cells from two hiPS cell lines derived from two subjects; two-tailed Mann–Whitney, *P*=0.68). The center line shows the median, the box shows s.e.m. and the whiskers represent 10th and 90th percentiles. **c**, Barium current charge (control, *n*=11 cells from two hiPS cell lines derived from two subjects; 22q11DS, *n*=12 cells from two hiPS cell lines derived from two subjects; two-tailed Mann–Whitney, *P*=0.44). The center line shows the median, the box shows s.e.m. and the whiskers represent 10th and 90th percentiles. **d**, RMP in 22q11DS versus control neurons shown (left) per group and (right) per hiPS cell line (−43.18±0.84mV, *n*=60 neurons from 22q11DS neurons from six hiPS cell lines; −52.68±0.93mV, *n*=64 control neurons from four hiPS cell lines; two-tailed *t*-test, ****$P<0.0001$). The center line shows the median, the box shows s.e.m. and the whiskers represent the 10th and 90th percentiles. **e**, Example traces showing the effect of holding at −40mV or −70mV on calcium channel-mediated barium currents. **f**, The h∞ curve for all holding potentials (two-way repeated measures $F_{1,14}$=0.96, *P*=0.35 between groups). Inset: comparison of the fraction of available channels for control and 22q11DS at their respective RMPs (control, *n*=8 cells from two hiPS cell lines; 22q11DS, *n*=7 from two hiPS cell lines). Data (main plot) are presented as mean±s.e.m. In the inset, the center line shows the median, the box shows s.e.m. and the whiskers represent the 10th and 90th percentile. **g**, Example traces showing the effect of an inactivating voltage pre-pulse on Fura-2 ratio changes (left) and quantification of the inactivating pulse on the response amplitude (right) (*n*=9 cells; two-tailed, paired *t*-test, **$P=0.002$).

2D-derived 22q11DS and control neurons after labeling with AAV–Syn1::YFP (Extended Data Fig. 6e). We found that co-culturing did not affect the phenotype (Extended Data Fig. 6f; $P=0.008$).

We next sought to gain insight into the mechanism underlying the depolarization-induced $[Ca^{2+}]_i$ impairment in 22q11DS. To test whether the biophysical properties or the density of calcium channels could explain this phenotype, we performed voltage-clamp recordings from neurons. We first used $Ba^{2+}$ as the main charge carrier to reduce the effect of $Ca^{2+}$-dependent inactivation on the channels (Fig. 3a). In the presence of pharmacological agents that isolate calcium-channel-mediated currents, we found no difference in the $Ba^{2+}$ current amplitude or charge between 22q11DS and control hCS neurons (Fig. 3b,c; $P=0.68$ for amplitude; $P=0.44$ for charge) or 2D-derived cortical neurons (Extended Data Fig. 6h,i; $P=0.23$ for amplitude; $P=0.28$ for charge). We also found no significant difference in the activation curve between the groups (Extended Data Fig. 7g; $P=0.78$). Finally, using patch-clamp measurements with $Ca^{2+}$ as the charge carrier, we did not find a reduction current amplitude or charge in 22q11DS neurons (Extended Data Fig. 6j,k; $P=0.04$). Together, these findings suggest that the calcium deficit in 22q11DS neurons is not caused by a reduction in either the LTCCs number or the activation kinetics.

We then considered the possibility that changes in the conductance of other ions might explain the excitability and calcium phenotype in 22q11DS. We measured the RMP and found that patient-derived neurons were more depolarized (Fig. 3d; $P<0.0001$). Although the variability across lines and interaction in the mixed model contributed 47% of the variance, the fixed effect was significant (Fig. 3d, right; $P<0.01$). Similarly, 2D cortical neurons from 22q11DS were also more depolarized (Extended Data Fig. 6g; $P=0.0005$). The electrophysiological properties of our hiPS cell–derived neurons are very similar to what has been previously reported in human neurons[38]. The RMP for control hiPS cell–derived neurons is approximately −52 mV. Similarly, recordings in slices of mid-gestation human cerebral cortex show an RMP of −49.8 mV (ref. [38]). Interestingly, altered excitability and a tendency towards depolarized RMP have also been observed at postnatal stages in pyramidal neurons in a 22q11DS rodent model[29,39].

We next inquired how changes in RMP could lead to the calcium defect in 22q11DS cortical neurons. One mechanism that controls LTCCs availability is voltage-dependent inactivation, which occurs on the timescale of seconds[40]. We calculated the inactivation curve (h∞) of control and 22q11DS neurons by holding the neurons at different holding potentials (−110 to +30 mV) for 5 s, before applying an activating step to −20 mV (Fig. 3e). We found no difference in the shape of the inactivation curve (Fig. 3f; $P=0.35$). However, the fraction of available channels at −50 mV and −40 mV, which roughly correspond to the RMP of control or 22q11DS neurons, respectively, was decreased in patients (Fig. 3f, inset).

To better understand the effect of voltage-dependent calcium channel inactivation, we induced a subtle depolarization in control neurons by pretreatment with 10 mM KCl prior to applying 67 mM KCl[41]. We found that the pretreatment (in 2D- and 3D-derived neurons) resulted in a decrease in the $[Ca^{2+}]_i$ amplitude in control neurons (~31%), partly mimicking the phenotype in 22q11DS (Extended Data Fig. 7h,i; hCS, $P<0.0001$; Extended Data Fig. 6l,m; 2D, $P<0.0001$). Finally, we directly tested how these changes in LTCC availability affect $[Ca^{2+}]_i$ rise by imaging patch-clamped neurons. We filled single, control-derived neurons with cell impermeant Fura-2 dye and performed calcium imaging while whole-cell voltage-clamping neurons (Fig. 3g, left). We found that the rise in $[Ca^{2+}]_i$ following a depolarizing voltage step from −70 mV to +10 mV was approximately two times lower when preceded by an inactivating pre-pulse to −40 mV (Fig. 3g, right; $P=0.02$). Taken together, these experiments suggest that voltage-dependent inactivation of calcium channels, which is related to a more depolarized membrane potential, results in a defect in $[Ca^{2+}]_i$ in 22q11DS neurons. Moreover, defects in RMP are also probably causing a change in excitability in 22q11DS neurons.

**Heterozygous loss of *DGCR8* recapitulates functional phenotypes of 22q11DS neurons.** One of the genes deleted in the 22q11.2 region, *DGCR8* (a component of the microprocessor complex involved in miRNA biogenesis[30]), has been associated with neuronal defects in rodent models of disease and therefore has an outsized potential to dysregulate downstream target genes contributing to neuronal phenotype[11,42]. To investigate if DGCR8 may be involved in the excitability and calcium phenotypes in human 22q11DS cortical neurons, we used CRISPR/Cas9 to induce a single-allele base-pair insertion and generate a heterozygous isogenic line ($DGCR8^{+/-}$) in a control background (Extended Data Fig. 9a).

In cell-attached patch-clamp recordings, we found that $DGCR8^{+/-}$ $Syn1^+$ cells were also approximately four times more likely to spontaneously fire APs than $Syn1^+$ cells derived from the parental hiPS cell line (Fig. 4a,b, $P=0.003$). We next investigated if abnormal neuronal excitability in $DGCR8^{+/-}$ neurons is coupled with changes in calcium signaling during depolarization. Using Fura-2 live imaging, we observed a decrease in the amplitude of $[Ca^{2+}]_i$ rise following depolarization (Fig. 4c), which was similar to the defects in 22q11DS neurons (Fig. 4d; $P<0.0001$). We also measured the RMP in patch-clamped cells and found that $DGCR8^{+/-}$-derived neurons were more depolarized than the parental control neurons (Fig. 4e; $P=0.009$). Overall, these results show that heterozygous loss of the *DGCR8* gene in hiPS cell derived neurons is sufficient to induce changes in calcium and excitability in 22q11DS cortical neurons.

**Genetic rescue of defects in 22q11DS neurons.** To explore the role of DGCR8 in mediating calcium defects in cortical neurons and to assess the reversibility of these phenotypes, we first attempted to rescue phenotypes in $DGCR8^{+/-}$ hCSs by acute gene replacement. We delivered *DGCR8* using a lentiviral construct (Lenti–EF1α::*DGCR8*) in $DGCR8^{+/-}$ neurons at days 60–70 (Extended Data Fig. 9b). Imaging with Fura-2 at days 70–80 showed that overexpression of *DGCR8* restored the amplitude of $[Ca^{2+}]_i$ rise following depolarization (Fig. 5a,b; $P=0.002$). Interestingly, overexpression of *DGCR8* in control cells did not result in a higher amplitude of $[Ca^{2+}]_i$ rise following depolarization (Fig. 5b; $P>0.99$).

To determine if DGCR8 could rescue 22q11DS phenotypes, we overexpressed *DGCR8* in hCS neurons differentiated from two patients with 22q11DS (Extended Data Fig. 9c). Imaging with Fura-2 showed that overexpression increased the amplitude of $[Ca^{2+}]_i$ rise following depolarization, although it did not restore the amplitude to control levels (Fig. 5c,d and Extended Data Fig. 9c). To explore potential transcriptional overlap between $DGCR8^{+/-}$ and 22q11DS neurons, we used quantitative polymerase chain reaction with reverse transcription (RT-qPCR) to test the expression of eight selected 22q11DS DEG genes that are related to ion transport (*ATP1A2*, *CACNB4*, *KCNJ11*, *CALY*) and excitability (*WNT5A*, *PCP4*, *CALCB*), as well as one of the top DEG genes, *ZNF132*. We found that *ATP1A2*[43] (a sodium-potassium transporter ATPase involved in maintaining the RMP), *WNT5A* (which regulates neuronal excitability and calcium signaling in development[44]) and *ZNF132* were also downregulated in $DGCR8^{+/-}$ hCSs (Extended Data Fig. 9d). These results indicate that acute overexpression of *DGCR8* in human cortical neurons that are heterozygous for *DGCR8* or the 22q11.2 locus can lead to partial rescue in calcium signaling, suggesting a potential role for DGCR8 in regulating neuronal excitability.

Finally, we examined the effect of DGCR8 overexpression on the RMP of 22q11DS and control neurons. We found that at 10–15 days following viral delivery, DGCR8 overexpression hyperpolarized the membrane potential of 22q11DS neurons by ~7 mV, while it had little or no effect in control neurons (Fig. 5e; $P=0.01$).

**Pharmacological rescue of functional defects in 22q11DS neurons.** One way to ascertain disease-relevant phenotypes is to identify cellular phenomena that can be reversed with drugs that can improve clinical symptoms. Current evidence suggests that individuals with 22q11DS respond similarly to individuals with idiopathic SCZ when treated with antipsychotics[45,46]. A common feature of many antipsychotics is a modulation of DA D2 receptor function, which has been linked to clinical response[46,47]. This $G_{\alpha i}$ coupled receptor has been shown to modulate the function of LTCCs[48,49]. Previous work has reported expression of the *DRD2* gene, which encodes the D2 receptor, in pyramidal neurons of the cortex in vivo[49,50]. We found that the D2 receptor is expressed by at least a subset of hiPS cell–derived cortical neurons, similar to what has been reported in vivo[49,50] (Extended Data Fig. 10a,b). Therefore, we exposed 22q11DS neurons to raclopride, a high-affinity D2 receptor blocker[51], and imaged $[Ca^{2+}]_i$ shortly before and during depolarization (Fig. 6a,b). We found that pretreatment with raclopride was sufficient to restore the deficit in $[Ca^{2+}]_i$ in 22q11DS neurons, while having no statistically significant effect on control neurons (Fig. 6a,b; $P<0.003$). On average, raclopride increased the $[Ca^{2+}]_i$ amplitude by ~104% in 22q11DS. Using cell-attached patch-clamp recordings, we also found a reduction in the fraction of spontaneously firing 22q11DS neurons after application of raclopride (Fig. 6c; $P=0.03$; $P=0.37$). Additionally, raclopride pretreatment was sufficient to restore the deficit in $[Ca^{2+}]_i$ in $DGCR8^{+/-}$ neurons (Fig. 6d,e; $P<0.0001$).

To verify that this effect was not restricted to raclopride, we tested another antipsychotic. We found that pretreatment with sulpiride was sufficient bring the 22q11DS $[Ca^{2+}]_i$ amplitude to control levels (Extended Data Fig. 10c,d; $P=0.008$).

Next, we wondered whether the rescue effect by raclopride or sulpiride was mediated by a change in the RMP. We used patch clamping to monitor RMP changes of the neurons (held at −40 mV) while applying raclopride using a local puff electrode. We found that, within seconds, raclopride application resulted in hyperpolarization by ~5 mV in both control and 22q11DS cells (Fig. 6f; for

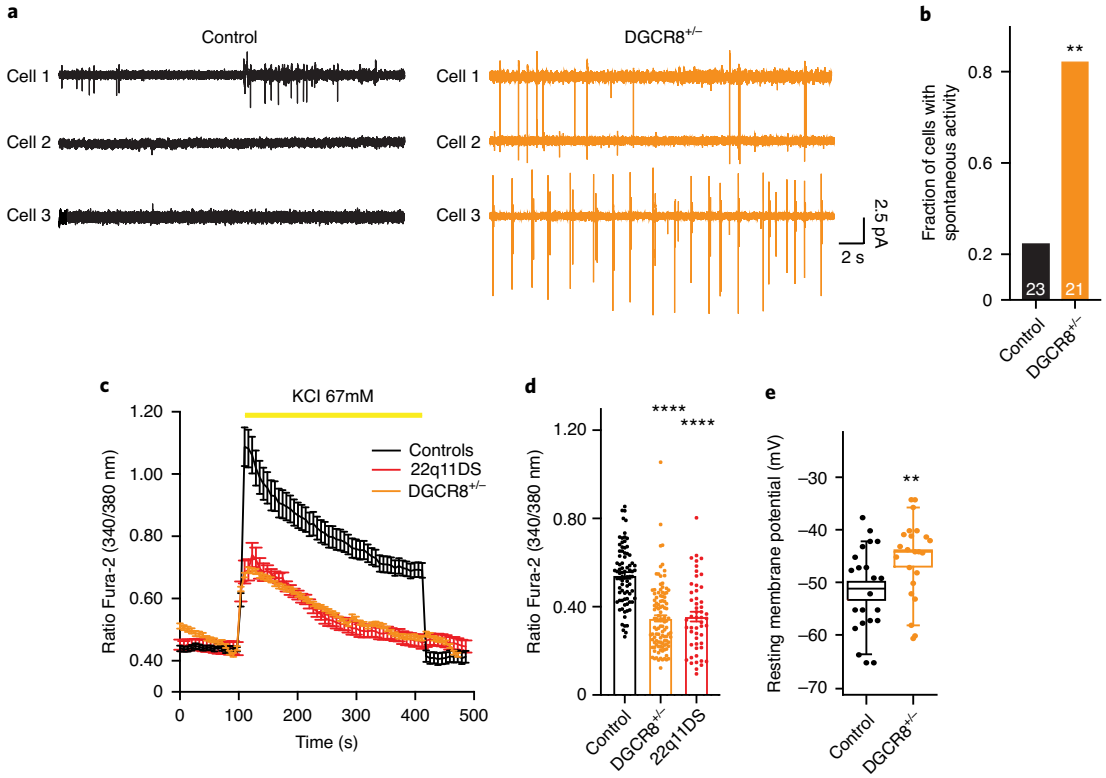


**Fig. 4 | Heterozygous loss of *DGCR8* recapitulates functional phenotypes of 22q11DS neurons. a**, Representative traces show spontaneous APs recorded in cell-attached mode from control and DGCR8$^{+/-}$ neurons. **b**, The fraction of cells with spontaneous APs ($n=21$ cells for DGCR8$^{+/-}$ versus $n=23$ cells for isogenic control, chi-squared test for proportion of cells, $\chi^2=8.31$, $^{**}P=0.003$). **c**, Changes in Fura-2 in response to 67 mM KCl in control and DGCR8$^{+/-}$ neurons (isogenic control, $n=35$ cells from one hiPS cell line; 22q11DS, $n=20$ cells from two hiPS cell lines; DGCR8$^{+/-}$, $n=54$ cells from one isogenic hiPS cell line). Data are presented as mean ratio ± s.e.m. **d**, Quantification of KCl-induced Fura-2 amplitude (isogenic control, $n=80$ cells from one hiPS cell line; 22q11DS, $n=53$ cells from two hiPS cell lines; DGCR8$^{+/-}$, $n=109$ cells from one hiPS cell line, two-tailed Kruskal–Wallis test, $P<0.0001$; following Dunn's multiple comparison test, $^{****}P<0.0001$ for DGCR8$^{+/-}$ versus parental control, $^{****}P<0.0001$ for 22q11DS versus parental control; $P>0.99$ DGCR8$^{+/-}$ versus 22q11DS). Data are presented as mean peak amplitude ± s.e.m. **e**, RMP in control and DGCR8$^{+/-}$ neurons (−51.4 ± 1.72 mV, $n=21$ isogenic control neurons versus −45.16 ± 1.55 mV, $n=23$ DGCR8$^{+/-}$ neurons; two-tailed *t*-test, $^{**}P=0.009$). The center line shows the median, the box shows s.e.m. and the whiskers represent the 10th and 90th percentile.

22q11DS, $P=0.01$; for control, $P=0.004$). Similarly, we found that the application of sulpiride resulted in hyperpolarization of control and 22q11DS neurons (Extended Data Fig. 10e; 22q11DS, $P=0.002$; control, $P<0.0001$). Finally, we tested a second-generation antipsychotic drug that has lower affinity for DA D2 receptors[52]. We found that the application of olanzapine, at a similar concentration, also resulted in hyperpolarization and rescue of the RMP of 22q11DS neurons (Extended Data Fig. 10f; $P=0.008$). These data suggest that these three antipsychotic drugs probably rescue the 22q11DS defect by restoring the RMP in cortical neurons.

## Discussion

Microdeletions at the 22q11.2 locus are the most frequent interstitial deletion in humans[53]. The clinical phenotype of 22q11DS is highly variable and involves multiple systems. Although the cardiovascular and immune deficiencies can be managed successfully in 22q11DS, the associated psychiatric disorders remain unaddressed therapeutically. This is partly because the molecular defects underlying neurodevelopmental disorders in 22q11DS are not known. Previous models for this disease have provided pathophysiological clues[9,10,54], but we are still far from developing effective therapeutics for mental illness in 22q11DS.

Using both cortical organoids and 2D glutamatergic neurons from a large cohort of patients with 22q11DS and controls, we identified specific cellular phenotypes associated with 22q11DS. Although the defect was observed in both 2D and 3D cortical neurons, derivation of hCSs allowed us to scale up neural differentiation experiments, as we have previously found[22]. Importantly, we showed that neural differentiations are highly reliable and 22q11DS is not associated with major defects in corticogenesis. Starting with transcriptional profiling of cortical neurons, we first identified a signature suggestive of perturbed neural excitability. Electrophysiological and imaging experiments confirmed an increase in excitability and impaired depolarization-induced LTCC calcium signaling in 22q11DS-derived neurons, which were related to a defect in the RMP that caused voltage-dependent inactivation of calcium channels. Although we showed that this phenotype was present up to 5.5 months, it remains to be established whether 22q11DS neurons will recover following maturation, homeostatic events or integration into circuits with interneurons. Moreover, future studies should elucidate if this excitability defect is related to the higher prevalence of seizures in 22q11DS[55]. Nonetheless, such changes could shape the formation of cortical circuits and contribute to disease susceptibility. Interestingly, in vitro treatment with the antipsychotics raclopride, sulpiride and olanzapine, which modulate neuronal excitability[51,56,57], rescued the RMP deficit. Several reports have now confirmed an association between the LTCC *CACNA1C* gene and neurodevelopmental disorders[25,58]. Interestingly, in contrast to the

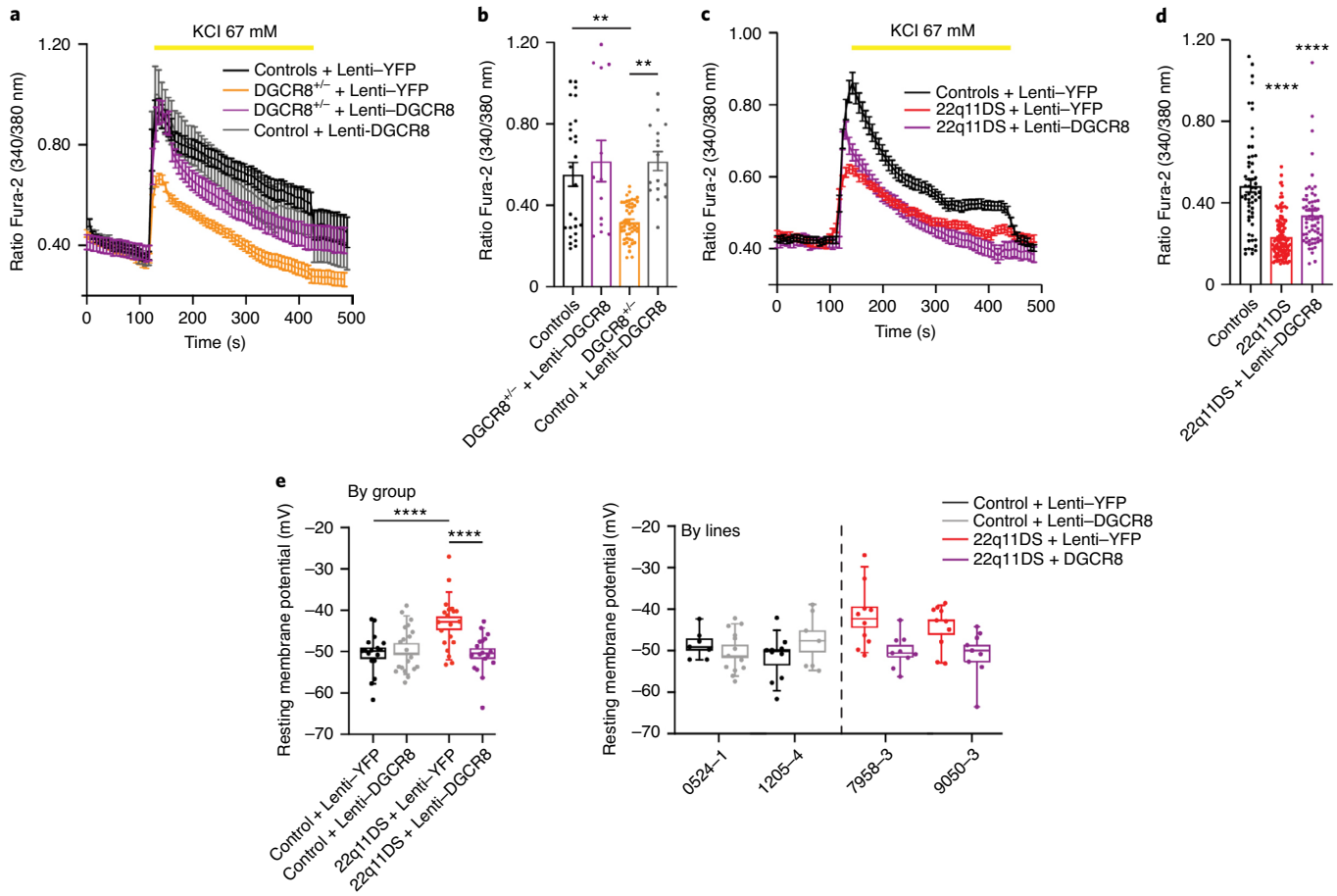


**Fig. 5 | Genetic rescue of phenotypes in 22q11DS neurons. a**, Depolarization-induced changes in Fura-2 ratio following overexpression of DGCR8 (Lenti-EF1α::DGCR8-YFP+) in control and DGCR8$^{+/-}$ neurons (isogenic control, $n=26$ cells from one hiPS cell line; DGCR8$^{+/-}$, $n=50$ from one control hiPS cell line derived from the isogenic control; isogenic control + Lenti-DGCR8, $n=13$ cells from one hiPS cell line derived; DGCR8$^{+/-}$ + Lenti-DGCR8, $n=16$ cells derived from the isogenic control). Data are presented as mean ratio ± s.e.m. **b**, Quantification of peak $[Ca^{2+}]_i$ amplitude from **a** (two-way ANOVA for DGCR8 overexpression, $F_{1,81}=10.16$, $^{**}P=0.002$; Tukey's multiple comparison test, $^{**}P=0.003$ for DGCR8$^{+/-}$ + Lenti-DGCR8 versus DGCR8$^{+/-}$; $P=0.82$ for DGCR8$^{+/-}$ + Lenti-DGCR8 versus control; $^{**}P=0.005$ for DGCR8$^{+/-}$ versus isogenic control). Data are presented as mean peak amplitude ± s.e.m. **c**, Depolarization-induced changes in Fura-2 ratio following overexpression of *DGCR8* (Lenti-EF1α::DGCR8-YFP+) in 22q11DS neurons (control, $n=59$ cells from three hiPS cell lines derived from three subjects; 22q11DS, $n=118$ cells from two hiPS cell lines derived from two subjects; 22q11DS + Lenti-DGCR8, $n=64$ cells from two 22q11DS hiPS cell lines derived from two subjects). Data are presented as mean ratio ± s.e.m. **d**, Quantification of peak $[Ca^{2+}]_i$ amplitude from **b** (two-tailed Kruskal–Wallis test, $P<0.0001$; following Dunn's multiple comparison test, $^{****}P<0.0001$ for 22q11DS + Lenti-DGCR8 versus 22q11DS, $P=0.007$ for 22q11DS + Lenti-DGCR8 versus control; $^{****}P<0.0001$ for 22q11DS versus control). Data are presented as mean peak amplitude ± s.e.m. **e**, The effect of DGCR8 overexpression (Lenti-EF1α::DGCR8-YFP) on the RMP of control and 22q11DS neurons (control + Lenti-YFP, $n=17$ cells from two hiPS cell lines derived from two subjects; control + Lenti-DGCR8, $n=20$ cells from two hiPS cell lines derived from two subjects; 22q11DS + Lenti-YFP, $n=20$ cells from two hiPS cell lines from two subjects; 22q11DS + Lenti-DGCR8, $n=18$ cells from two hiPS cell lines derived from two subjects; two-way ANOVA for DGCR8 overexpression, $F_{1,71}=6.05$, $P=0.01$; Tukey's multiple comparison test, $^{****}P<0.0001$ for 22q11DS + Lenti-YFP versus 22q11DS + Lenti-DGCR8, $^{****}P<0.0001$ for 22q11DS + Lenti-YFP versus control + Lenti-YFP). The center lines shows the median, the box shows s.e.m. and whiskers represent the 10th and 90th percentiles.

reduced $[Ca^{2+}]_i$ in 22q11DS, we recently reported increased $[Ca^{2+}]_i$ in Timothy syndrome, a monogenic ASD[23]. Alterations in both LTCC functions can be rescued efficiently within minutes by the antipsychotics. The modulation of LTCCs by D2 receptors in neurons is well established, and blocking of D2 receptors can increase the activity of LTCCs via multiple pathways[27,48]. Owing to their inverse agonist effects[59], these drugs could also decrease the tonic signaling from DA receptors in the absence of DA or, especially in the case of second-generation drugs such as olanzapine, exert an effect on excitability by modulating non-dopaminergic receptors such as 5-HT receptors[60]. Finally, we note that this class of drugs has complex effects on neurons and that hyperpolarization rescue may be unrelated to antipsychotic response in patients.

We found that heterozygous loss of *DGCR8* is sufficient to phenocopy the functional defect in 22q11DS neurons. Interestingly, we observed only a modest reduction in the miRNA-processing *DGCR8* gene in 22q11DS neurons. However, several studies have reported less than expected downregulation of *DGCR8* mRNA in heterozygous cell lines, which is thought to be due to homeostatic mechanisms. *DGCR8* works in a complex with an RNAse, *DROSHA*, and regulates the expression of many transcripts[30]. Thereby, any level of alteration in DGCR8 would presumably have downstream effects on protein production and, potentially, neuronal physiology. Exogenously expressing *DGCR8* rescued these defects in an isogenic line but only partially in 22q11DS. Future studies should comprehensively investigate the transcriptional overlap between

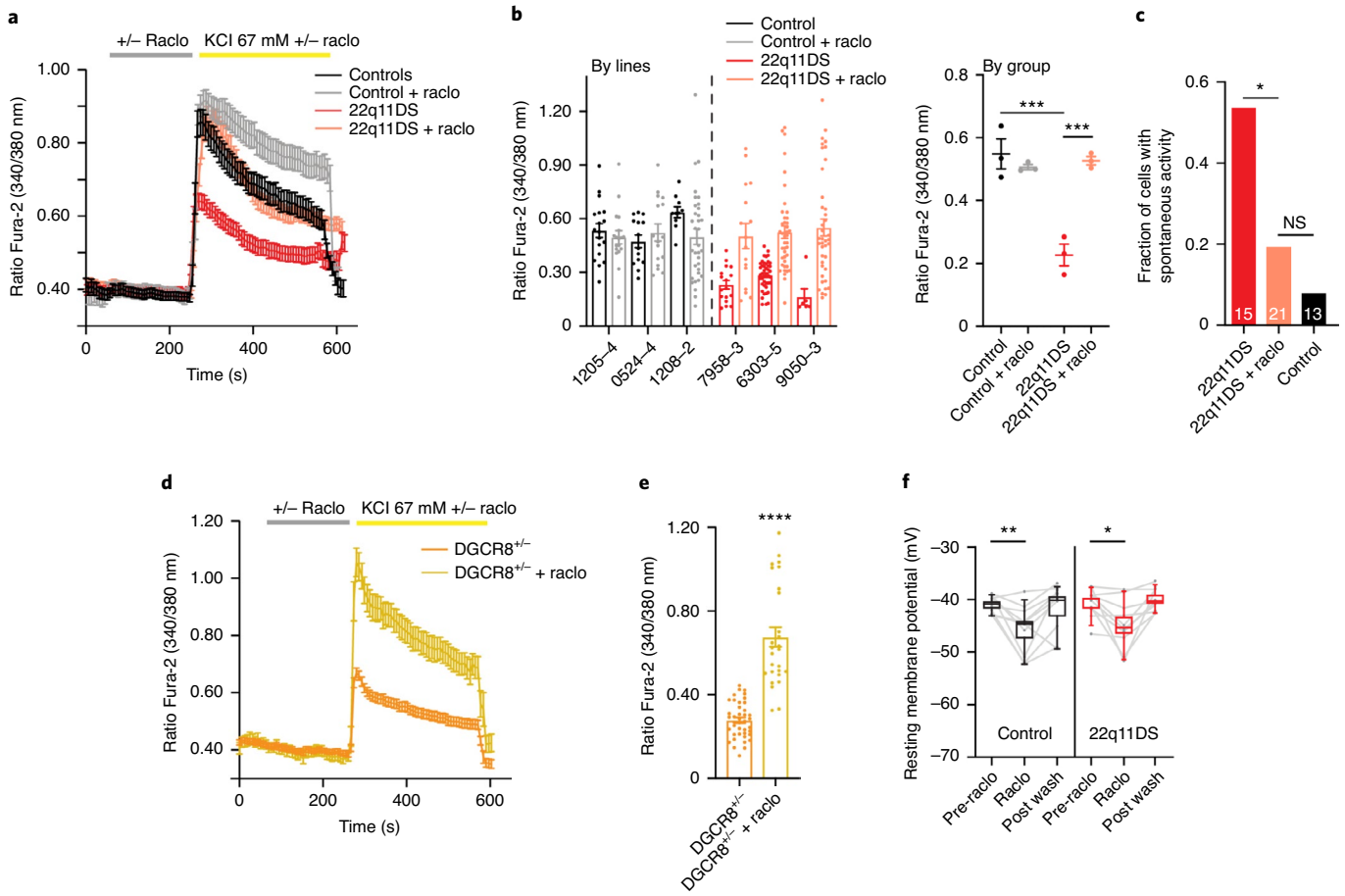


**Fig. 6 | Pharmacological modulation of phenotypes in 22q11DS neurons. a**, Changes in Fura-2 in response to 67 mM KCl in the presence or absence of raclopride (control, $n=42$ cells from three hiPS cell lines derived from three subjects; 22q11DS, $n=66$ cells from two hiPS cell lines derived from three subjects; control + raclopride, $n=68$ cells from three control hiPS cell lines derived from three subjects; 22q11DS + raclopride, $n=98$ cells from three hiPS cell lines derived from three subjects). Data are presented as mean ratio ± s.e.m. **b**, Quantification of Fura-2 amplitude from **a** (two-way ANOVA for raclopride exposure $F_{1,8}=17.83$, $^{**}P<0.003$; Tukey's multiple comparison test, $^{***}P=0.0005$ for 22q11DS versus 22q11DS + raclopride; $P=0.96$ for 22q11DS + raclopride versus control; $P=0.76$ for control versus control + raclopride; $^{***}P=0.0003$ for 22q11DS versus control). A 2-min pretreatment was given before the raclopride addition. Data are presented as mean peak amplitude ± s.e.m. **c**, Fraction of 22q11DS neurons with spontaneous APs following raclopride application ($n=15$ for 22q11DS Syn1$^+$ neurons versus $n=21$ for 22q11DS + raclopride, chi-squared test for proportion of cells, $\chi^2=4.5$, $^{*}P=0.03$; $n=13$ Syn1$^+$ control neurons versus 22q11DS + raclopride, chi-squared test for proportion of cells, $\chi^2=0.8$, $P=0.37$; NS, not significant). **d**, The effect of raclopride on Fura-2 ratio changes in response to KCl application in DGCR8$^{+/-}$ and isogenic control neurons (isogenic control, $n=41$ cells from one hiPS cell line; DGCR8$^{+/-}$, $n=27$ cells from one isogenic hiPS cell line). Data are presented as mean ratio ± s.e.m. **e**, Quantification of the effect of raclopride on Fura-2 ratio amplitude in DGCR8$^{+/-}$ neurons (two-tailed Mann–Whitney test, $^{****}P<0.0001$). A 2-min pretreatment was given before raclopride addition. Data are presented as mean peak amplitude ± s.e.m. **f**, The effect of raclopride on the RMP of control and 22q11DS neurons ($n=10$ control neurons from two hiPSC cell lines derived from two subjects, one-way repeated measures ANOVA, $F_{2,18}=7.4$, $^{**}P=0.004$, Tukey's multiple comparisons test, $^{**}P=0.006$ for pre-raclopride versus raclopride, $^{*}P=0.01$ for raclopride versus post-wash, $P=0.91$ for pre-raclopride versus post-wash; $n=10$ 22q11DS cells from two hiPSC cell lines derived from two subjects, one-way repeated measures ANOVA, $F_{2,18}=9.71$, $^{*}P=0.01$, Tukey's multiple comparisons test, $^{**}P=0.007$ for pre-raclopride versus raclopride, $^{**}P=0.002$ for raclopride versus post-wash and $P=0.8$ for pre-raclopride versus post-wash). The center line shows the median, the box shows s.e.m. and the whiskers represent the 10th and 90th percentiles.

22q11DS and DGCR8$^{+/-}$ and identify the miRNA(s) that may lead to the above functional changes. Additionally, it remains to be seen whether any other regulatory 22q11.2 locus regions influence these deficits. Finally, the genomic complexity of this disease makes it likely that other genes in the locus contribute to these neuronal defects.

Overall, the transcriptional and physiological data in 22q11DS neurons suggest a link at the cellular level between several pathways that have been independently associated with neurodevelopmental disorders in previous studies. Moreover, transcriptional changes in 22q11DS neurons are also enriched for genes associated with increased risk for SCZ and ASD. It is therefore possible that, similar to 22q11DS, other disorders on the SCZ or autism spectrum may display convergence of multiple signaling defects in pathways suggested by GWAS.

Despite the variable clinical phenotypic expression in the 22q11DS group, the cellular phenotypes were robust and reproducible across subjects and lines. Our analyses in hiPS cell–derived neurons focused on identifying molecular or cellular features specific to 22q11.2 deletion instead of the associated clinical phenotypes. Larger samples are needed to reliably estimate genotype–phenotype associations. Given the distinct clinical phenotypes of SCZ and ASD, it will be interesting to expand this work in a larger sample to determine whether one can distinguish molecular pathways unique

to each clinical condition, as well as to identify the potential contribution of genetic background, including polygenic risk for SCZ. Future studies should also identify the molecular mechanism downstream of DGCR8 that leads to these cellular phenotypes, as well as the role for pharmacological modulation by antipsychotics.

By identifying disease-relevant cellular phenotypes and demonstrating convergence at the cellular level of multiple pathways associated independently with neurodevelopmental disorders, we provide novel insights into the neurobiological pathways underlying the development of mental illness in 22q11DS. These findings support the value of a major mutational model for elucidating the biology of complex neuropsychiatric disorders and open the avenue for uncovering therapeutics.

## Online content

Any methods, additional references, Nature Research reporting summaries, source data, extended data, supplementary information, acknowledgements, peer review information; details of author contributions and competing interests; and statements of data and code availability are available at https://doi.org/10.1038/s41591-020-1043-9.

Received: 27 November 2019; Accepted: 30 July 2020;
Published online: 28 September 2020

## References

1. Sullivan, P. F., Daly, M. J. & O'Donovan, M. Genetic architectures of psychiatric disorders: the emerging picture and its implications. *Nat. Rev. Genet.* **13**, 537–551 (2012).
2. Sanders, S. J. et al. A framework for the investigation of rare genetic disorders in neuropsychiatry. *Nat. Med.* **25**, 1477–1487 (2019).
3. Zinkstok, J. R. et al. Neurobiological perspective of 22q11.2 deletion syndrome. *Lancet Psychiatry* **6**, 951–960 (2019).
4. Murphy, K. C., Jones, L. A. & Owen, M. J. High rates of schizophrenia in adults with velo-cardio-facial syndrome. *Arch. Gen. Psychiatry* **56**, 940–945 (1999).
5. Monks, S. et al. Further evidence for high rates of schizophrenia in 22q11.2 deletion syndrome. *Schizophr. Res.* **153**, 231–236 (2014).
6. Schneider, M. et al. Psychiatric disorders from childhood to adulthood in 22q11.2 deletion syndrome: results from the International Consortium on Brain and Behavior in 22q11.2 Deletion Syndrome. *Am. J. Psychiatry* **171**, 627–639 (2014).
7. Vorstman, J. A. et al. The 22q11.2 deletion in children: high rate of autistic disorders and early onset of psychotic symptoms. *J. Am. Acad. Child Adolesc. Psychiatry* **45**, 1104–1113 (2006).
8. Olsen, L. et al. Prevalence of rearrangements in the 22q11.2 region and population-based risk of neuropsychiatric and developmental disorders in a Danish population: a case-cohort study. *Lancet Psychiatry* **5**, 573–580 (2018).
9. Drew, L. J. et al. The 22q11.2 microdeletion: fifteen years of insights into the genetic and neural complexity of psychiatric disorders. *Int. J. Dev. Neurosci.* **29**, 259–281 (2011).
10. Karayiorgou, M., Simon, T. J. & Gogos, J. A. 22q11.2 microdeletions: linking DNA structural variation to brain dysfunction and schizophrenia. *Nat. Rev. Neurosci.* **11**, 402–416 (2010).
11. Chun, S. et al. Specific disruption of thalamic inputs to the auditory cortex in schizophrenia models. *Science* **344**, 1178–1182 (2014).
12. Sigurdsson, T., Stark, K. L., Karayiorgou, M., Gogos, J. A. & Gordon, J. A. Impaired hippocampal-prefrontal synchrony in a genetic mouse model of schizophrenia. *Nature* **464**, 763–767 (2010).
13. Fernandez, A. et al. Mitochondrial dysfunction leads to cortical under-connectivity and cognitive impairment. *Neuron* **102**, 1127–1142 e1123 (2019).
14. Demaerel, W. et al. The 22q11 low copy repeats are characterized by unprecedented size and structural variability. *Genome Res.* **29**, 1389–1401 (2019).
15. Pasca, S. P. The rise of three-dimensional human brain cultures. *Nature* **553**, 437–445 (2018).
16. Zhao, D. et al. MicroRNA profiling of neurons generated using induced pluripotent stem cells derived from patients with schizophrenia and schizoaffective disorder, and 22q11.2 Del. *PLoS ONE* **10**, e0132387 (2015).
17. Toyoshima, M. et al. Analysis of induced pluripotent stem cells carrying 22q11.2 deletion. *Transl. Psychiatry* **6**, e934 (2016).
18. Lin, M. et al. Integrative transcriptome network analysis of iPSC-derived neurons from schizophrenia and schizoaffective disorder patients with 22q11.2 deletion. *BMC Syst. Biol.* **10**, 105 (2016).
19. Pasca, A. M. et al. Functional cortical neurons and astrocytes from human pluripotent stem cells in 3D culture. *Nat. Methods* **12**, 671–678 (2015).
20. Sloan, S. A., Andersen, J., Pasca, A. M., Birey, F. & Pasca, S. P. Generation and assembly of human brain region-specific three-dimensional cultures. *Nat. Protoc.* **13**, 2062–2085 (2018).
21. Sloan, S. A. et al. Human astrocyte maturation captured in 3D cerebral cortical spheroids derived from pluripotent stem cells. *Neuron* **95**, 779–790 (2017).
22. Yoon, S. J. et al. Reliability of human cortical organoid generation. *Nat. Methods* **16**, 75–78 (2019).
23. Paşca, S. P. et al. Using iPSC-derived neurons to uncover cellular phenotypes associated with Timothy syndrome. *Nat. Med.* **17**, 1657–1662 (2011).
24. Sun, Y. et al. A deleterious Nav1.1 mutation selectively impairs telencephalic inhibitory neurons derived from Dravet syndrome patients. *eLife* **5**, e13073 (2016).
25. Cross-Disorder Group of the Psychiatric Genomics Consortium. Identification of risk loci with shared effects on five major psychiatric disorders: a genome-wide analysis. *Lancet* **381**, 1371–1379 (2013).
26. Moskvina, V. et al. Gene-wide analyses of genome-wide association data sets: evidence for multiple common risk alleles for schizophrenia and bipolar disorder and for overlap in genetic risk. *Mol. Psychiatry* **14**, 252–260 (2009).
27. Yasumoto, F. et al. Dopamine receptor 2 regulates L-type voltage-gated calcium channel in primary cultured mouse midbrain neural network. *Cell. Mol. Neurobiol.* **24**, 877–882 (2004).
28. Morrow, B. E., McDonald-McGinn, D. M., Emanuel, B. S., Vermeesch, J. R. & Scambler, P. J. Molecular genetics of 22q11.2 deletion syndrome. *Am. J. Med. Genet. A* **176**, 2070–2081 (2018).
29. Sun, Z., Williams, D. J., Xu, B. & Gogos, J. A. Altered function and maturation of primary cortical neurons from a 22q11.2 deletion mouse model of schizophrenia. *Transl. Psychiatry* **8**, 85 (2018).
30. Han, J. et al. The Drosha–DGCR8 complex in primary microRNA processing. *Genes Dev.* **18**, 3016–3027 (2004).
31. Gokhale, A. et al. Systems analysis of the 22q11.2 microdeletion syndrome converges on a mitochondrial interactome necessary for synapse function and behavior. *J. Neurosci.* **39**, 3561–3581 (2019).
32. Grove, J. et al. Identification of common genetic risk variants for autism spectrum disorder. *Nat. Genet.* **51**, 431–444 (2019).
33. Pardinas, A. F. et al. Common schizophrenia alleles are enriched in mutation-intolerant genes and in regions under strong background selection. *Nat. Genet.* **50**, 381–389 (2018).
34. Demontis, D. et al. Discovery of the first genome-wide significant risk loci for attention deficit/hyperactivity disorder. *Nat. Genet.* **51**, 63–75 (2019).
35. Parikshak, N. N. et al. Genome-wide changes in lncRNA, splicing, and regional gene expression patterns in autism. *Nature* **540**, 423–427 (2016).
36. Fromer, M. et al. Gene expression elucidates functional impact of polygenic risk for schizophrenia. *Nat. Neurosci.* **19**, 1442–1453 (2016).
37. Krey, J. F. et al. Timothy syndrome is associated with activity-dependent dendritic retraction in rodent and human neurons. *Nat. Neurosci.* **16**, 201–209 (2013).
38. Moore, A. R. et al. Electrical excitability of early neurons in the human cerebral cortex during the second trimester of gestation. *Cereb. Cortex* **19**, 1795–1805 (2009).
39. Drew, L. J. et al. Evidence for altered hippocampal function in a mouse model of the human 22q11.2 microdeletion. *Mol. Cell Neurosci.* **47**, 293–305 (2011).
40. Zamponi, G. W., Striessnig, J., Koschak, A. & Dolphin, A. C. The physiology, pathology and pharmacology of voltage-gated calcium channels and their future therapeutic potential. *Pharm. Rev.* **67**, 821–870 (2015).
41. Wheeler, D. G. et al. $Ca_V1$ and $Ca_V2$ channels engage distinct modes of $Ca^{2+}$ signaling to control CREB-dependent gene expression. *Cell* **149**, 1112–1124 (2012).
42. Schofield, C. M. et al. Monoallelic deletion of the microRNA biogenesis gene Dgcr8 produces deficits in the development of excitatory synaptic transmission in the prefrontal cortex. *Neural Dev.* **6**, 11 (2011).
43. Gritz, S. M. & Radcliffe, R. A. Genetic effects of ATP1A2 in familial hemiplegic migraine type II and animal models. *Hum. Genomics* **7**, 8 (2013).
44. McQuate, A., Latorre-Esteves, E. & Barria, A. A Wnt/calcium signaling cascade regulates neuronal excitability and trafficking of NMDARs. *Cell Rep.* **21**, 60–69 (2017).
45. Bassett, A. S. & Chow, E. W. Schizophrenia and 22q11.2 deletion syndrome. *Curr. Psychiatry Rep.* **10**, 148–157 (2008).
46. Seeman, P., Lee, T., Chau-Wong, M. & Wong, K. Antipsychotic drug doses and neuroleptic/dopamine receptors. *Nature* **261**, 717–719 (1976).
47. Kapur, S., Zipursky, R., Jones, C., Remington, G. & Houle, S. Relationship between dopamine $D_2$ occupancy, clinical response and side effects: a double-blind PET study of first-episode schizophrenia. *Am. J. Psychiatry* **157**, 514–520 (2000).

48. Hernandez-Lopez, S. et al. $D_2$ dopamine receptors in striatal medium spiny neurons reduce L-type $Ca^{2+}$ currents and excitability via a novel PLCβ1-$IP_3$-calcineurin-signaling cascade. *J. Neurosci.* **20**, 8987–8995 (2000).
49. Gee, S. et al. Synaptic activity unmasks dopamine $D_2$ receptor modulation of a specific class of layer V pyramidal neurons in prefrontal cortex. *J. Neurosci.* **32**, 4959–4971 (2012).
50. Santana, N., Mengod, G. & Artigas, F. Quantitative analysis of the expression of dopamine $D_1$ and $D_2$ receptors in pyramidal and GABAergic neurons of the rat prefrontal cortex. *Cereb. Cortex.* **19**, 849–860 (2009).
51. Perez, M. F., White, F. J. & Hu, X. T. Dopamine $D_2$ receptor modulation of $K^+$ channel activity regulates excitability of nucleus accumbens neurons at different membrane potentials. *J. Neurophysiol.* **96**, 2217–2228 (2006).
52. Gardner, D. M., Baldessarini, R. J. & Waraich, P. Modern antipsychotic drugs: a critical overview. *CMAJ* **172**, 1703–1711 (2005).
53. Kobrynski, L. J. & Sullivan, K. E. Velocardiofacial syndrome, DiGeorge syndrome: the chromosome 22q11.2 deletion syndromes. *Lancet* **370**, 1443–1452 (2007).
54. Chun, S., Bayazitov, I. T., Blundon, J. A. & Zakharenko, S. S. Thalamocortical long-term potentiation becomes gated after the early critical period in the auditory cortex. *J. Neurosci.* **33**, 7345–7357 (2013).
55. Eaton, C. B. et al. Epilepsy and seizures in young people with 22q11.2 deletion syndrome: prevalence and links with other neurodevelopmental disorders. *Epilepsia* **60**, 818–829 (2019).
56. Yu, N., Tucker, K. R., Levitan, E. S., Shepard, P. D. & Canavier, C. C. Implications of cellular models of dopamine neurons for schizophrenia. *Prog. Mol. Biol. Transl. Sci.* **123**, 53–82 (2014).
57. Anwar, I. J., Miyata, K. & Zsombok, A. Brain stem as a target site for the metabolic side effects of olanzapine. *J. Neurophysiol.* **115**, 1389–1398 (2016).
58. Schizophrenia Working Group of the Psychiatric Genomics Consortium. Biological insights from 108 schizophrenia-associated genetic loci. *Nature* **511**, 421–427 (2014).
59. Akam, E. & Strange, P. G. Inverse agonist properties of atypical antipsychotic drugs. *Biochem. Pharmacol.* **67**, 2039–2045 (2004).
60. Li, P., Snyder, G. L. & Vanover, K. E. Dopamine targeting drugs for the treatment of Schizophrenia: past, present and future. *Curr. Top. Med. Chem.* **16**, 3385–3403 (2016).

## Methods

**Reprogramming and hiPS cell culture.** Human fibroblast cells were reprogrammed using the Sendai virus-based CytoTune iPS 2.0 kit (CytoTune 2.0, Invitrogen, A16517). Fibroblasts were plated in six-well plates two days before transduction to achieve a density of $2\times10^5$ to $3\times10^5$ cells per well. Cells were then transduced with the indicated set of Sendai vectors at a multiplicity of infection of 5–5–3 (*KOS–Myc–Klf4*). Virus was removed after 24 h and cells were cultured in fibroblast medium with 10% FBS (Gibco, 16000-044) in Dulbecco's modified Eagle medium (DMEM; Gibco, 10569-010) for a total of seven days, with media changes every other day. On day 7 after transduction, cells were collected with TrypLE (Gibco, 16563-029) and plated in the fibroblast medium onto truncated recombinant human vitronectin (VTN-N, Gibco, A14700)-coated plates. The following day, fibroblast medium was changed to Essential 8 medium (Gibco, A1517001) and cells were fed daily until days 20–22. For further culture, individual colonies were manually dissected and transferred to fresh vitronectin-coated dishes. Once hiPS cell clones were established, they were routinely cultured on vitronectin-coated dishes in Essential 8 medium, and cells were split every 4–5 days using 0.5 mM EDTA (Invitrogen, 15575-020) as previously described[22]. hiPS cell clones/lines were also generated using retroviruses or non-integrating episomal vectors from fibroblasts (see Supplementary Table 2 for details). We did not observe any systematic differences between cells reprogrammed by the two methods. Lines from 22q11DS and control subjects were reprogrammed in batches.

Some of the hiPS cell lines used in this study have been extensively characterized previously[23,61] using immunostaining with anti-NANOG and TRA 2–49/6E antibodies, karyotyping, generation of teratoma in nude mice and mapping of viral integration sites (Extended Data Fig. 1a). Validation of hiPS cell integrity, including verification of genome integrity and deletion size by high-density SNP arrays for all hiPS cell lines, is shown in Extended Data Fig. 1b,c. Cultures were regularly tested for mycoplasma and maintained mycoplasma free.

A total of 43 hiPS cell lines were generated from 15 healthy subjects and 15 patients with 22q11DS. Approval for this study was obtained from the Stanford IRB panel and informed consent was obtained from all subjects.

hiPS cells were cultured as previously described[20,62]. Briefly, hiPS cells were cultured on inactivated mouse embryonic fibroblast feeders (EmbryoMax PMEF; Millipore) in hiPS cell medium containing DMEM/F12 (1:1, Life Technologies, 11330), knockout serum (20%, Life Technologies, 10828), non-essential amino acids (1 mM, Life Technologies, 11140), GlutaMax (1:200, Life Technologies, 35050), β-mercaptoethanol (0.1 mM, Sigma-Aldrich, M3148), penicillin and streptomycin (1:100, Life Technologies, 15070) and supplemented with fibroblast growth factor 2 (FGF2, 10 ng ml$^{-1}$ diluted in 0.1% BSA; R&D Systems). Alternately, feeder-free hiPS cells were maintained on six-well plates coated with recombinant human vitronectin (VTN–N, Gibco, A14700) in Essential 8 medium (Life Technologies, A1517001) and passaged with 0.5 mM EDTA (Life Technologies, 15575).

**Generation of hCSs from hiPS cells.** The generation of hCSs from hiPS cells was performed as previously described[19,20]. hiPS cell lines were randomly selected for differentiation from each genotype. To initiate the generation of hCS from hiPS cells cultured on feeders, intact hiPS cell colonies were lifted from the plates using dispase (0.35 mg ml$^{-1}$) and transferred to ultra-low-attachment plastic dishes (Corning) in hiPS cell medium supplemented with the two SMAD inhibitors dorsomorphin (5 µM, Sigma-Aldrich, P5499) and SB-431542 (10 µM, Tocris, 1614) and the ROCK inhibitor Y-27632 (10 µM, Selleckchem, S1049). For the first five days, the hiPS cell medium was changed every day and supplemented with dorsomorphin and SB-431542. On the sixth day in suspension, neural spheroids were transferred to neural medium containing neurobasal-A (Life Technologies, 10888), B-27 supplement without vitamin A (Life Technologies, 12587), GlutaMax (1:100, Life Technologies), penicillin and streptomycin (1:100, Life Technologies) and supplemented with the growth factors epidermal growth factor (EGF, 20 ng ml$^{-1}$; R&D Systems) and fibroblast growth factor 2 (FGF2, 20 ng ml$^{-1}$; R&D Systems) until day 24. From day 25 to day 42, the neural medium was supplemented with the growth factors brain-derived neurotrophic factor (BDNF, 20 ng ml$^{-1}$, Peprotech) and neurotrophin 3 (20 ng ml$^{-1}$, Peprotech) with medium changes every other day. From day 43 onward, hCSs were maintained in unsupplemented neurobasal-A medium (NM, Thermo Fisher, 1088022) with medium changes every 4–6 days.

For the generation of hCSs from hiPS cells cultured on feeder-free conditions, hiPS cells were incubated with Accutase (Innovate Cell Technologies, AT-104) at 37 °C for 7 min, dissociated into single cells, and seeded into AggreWell 800 plates (STEMCELL Technologies, 34815) at a density of $3\times10^6$ single cells per well in Essential 8 medium supplemented with the ROCK inhibitor Y-27632 (10 µM, Selleckchem, S1049). After 24 h, spheroids were collected from each microwell by firmly pipetting (with a cut end of a P1000 tip) medium in the well up and down and transferring it into ultra-low-attachment plastic dishes (Corning, 3262) in Essential 6 medium (Life Technologies, A1516401) supplemented with dorsomorphin (2.5 µM, Sigma-Aldrich, P5499) and SB-431542 (10 µM, Tocris, 1614). From day 2 to day 6, Essential 6 medium was changed every day and supplemented with dorsomorphin and SB-431542. From the sixth day in suspension, neural spheroids were transferred to neural medium and maintained as described above.

**2D neuronal differentiation.** The differentiation of hiPS cells into cortical neural progenitor cells and neurons was carried using a previously described and validated protocol[23]. Briefly, cellular aggregates were generated from hiPS cell colonies by enzymatic dissociation and kept in suspension for five days in hiPS cell media supplemented with two SMAD pathway inhibitors: dorsomorphin (Sigma-Aldrich, 10 µM) and SB-431542 (Tocris, 10 µM). On day 6 in vitro, cellular aggregates were plated on a polyornithine/laminin-rich substrate in neural medium (NM) containing neurobasal (Life Technologies, 10888), B-27 without vitamin A (Life Technologies, 12587), GlutaMax (1:100, Life Technologies) and 100 U ml$^{-1}$ penicillin and streptomycin (1:100, Life Technologies). The NM was supplemented with 20 ng ml$^{-1}$ FGF2 (R&D Systems) and 20 ng ml$^{-1}$ EGF (R&D Systems). After 10 days, neural rosettes were mechanically isolated and expanded in suspension as neurospheres for an additional seven days before the initiation of differentiation by replating, FGF2/EGF withdrawal and the addition of 20 ng ml$^{-1}$ BDNF (Peprotech, 450-02) and 20 ng ml$^{-1}$ NT3 (Peprotech, 450-03). The vast majority of neurons obtained with this protocol expressed cortical layer specific markers, as previously assessed by single-cell qPCR[23].

**Dissociation of hCSs.** For enzymatic dissociation of hCSs for culture in a monolayer, we used a previously published protocol with some modifications[7]. Briefly, hCSs were incubated for 15 min at 37 °C with 10 U ml$^{-1}$ papain (Worthington) and gently triturated using a P1000 pipette in 100% FBS (Life Technologies, 16000). Cells were centrifuged and resuspended in NM (centrifugation at 200*g* for 7 min) supplemented with BDNF, NT3 and, for the first 24 h, 10 µM Y-27632. The cells were plated on glass coverslips (15 mm, Warner Instruments, 640713) coated with poly-L-ornithine (50 µg ml$^{-1}$, Sigma-Aldrich, P3655) and laminin (5 µg ml$^{-1}$, Sigma-Aldrich, L2020) at a density of 150,000 cells per coverslip. Cells were infected with either AAV–DJ–hSyn1::YFP, AAV–DJ–hSyn1::mCherry or pLV–EF1α::hDGCR8–YFP, pLV_EF1α::YFP for two days for experiments.

**Cryopreservation.** The hCSs were fixed in 4% paraformaldehyde (PFA) overnight, washed in PBS and transferred to 30% sucrose for 2–3 days. Subsequently, they were rinsed and embedded in optimal cutting temperature (OCT) compound and 30% sucrose (1:1) embedded in OCT (Tissue–Tek OCT Compound 4583, Sakura Finetek) and stored at −80 °C. For immunofluorescence, 12–14-µm-thick sections were cut using a Leica cryostat.

**Immunocytochemistry.** Neurons plated on 15-mm coverslips (Warner Instruments) and grown in 24-well plates were fixed with 4% PFA in PBS for 10 min at room temperature. The coverslips were washed three times in PBS and incubated in blocking solution (3% BSA diluted in PBS, 0.3% Triton X-100 (Millipore Sigma, T9284-100ML), 10% NDS (Abcam, ab7475)) for 1 h. Samples were then incubated with the indicated primary antibodies for 3 h at room temperature, or overnight at 4 °C, and then washed three times in PBS at room temperature before incubation with secondary antibodies. Alexa Fluor dyes (Life Technologies) were used at 1:1,000 dilution and nuclei were visualized with Hoechst 33258 (dilution 1:10,000; Thermo Fisher Science, H3569) Samples were mounted for microscopy on glass coverslips, using Aquamount (Polysciences, 18606), and imaged on a Zeiss M1 Axioscope with a ×10, ×20, ×40 or ×63 objective. The following antibodies were used: anti-MAP2 (guinea pig, Synaptic Systems 188004, 1:1,000 dilution), anti-DRD2 (rabbit, Frontier Institute, D2R-Rb-Af960; previously Frontier Institute, D2R-Rb-Af750, 1:300 dilution), anti-VGLUT1 (rabbit, Synaptic Systems, 135302, 1:500 dilution) and anti-CTIP2 (rat, Abcam, AB18465, 1:300 dilution). See refs. [23,61] for details on immunostaining of hiPS cell lines. StemLight Pluripotency Antibody Kit (Cell Signaling Technology, 9656S, 1:200 dilution for all antibodies in kit) was used for OCT4, NANOG, SSEA-3, TRA-1-60 and TRA-2-49. Images were processed with Image J (Fiji, version 2.0.0-rc-90/152p).

**RT-qPCR.** At least three spheroids were combined for RNA extraction. Total RNA was isolated using the RNeasy mini kit and RNase-Free DNase set (Qiagen), and template complementary DNA was prepared by reverse transcription using the SuperScript III First-Strand Synthesis SuperMix for RT-qPCR (Life Technologies). qPCR was performed with SYBR Green (Roche) on a ViiA7 machine (Applied Biosystems, Life Technologies). Data were processed using the QuantStudio RT-qPCR software (v1.1, Applied Biosystems). Primers and sequences are listed in Supplementary Table 3. Data are presented as mean ± s.e.m., unless otherwise indicated.

**Genome editing of hiPS cells.** hiPS cells were electroporated in a solution containing 6 µg of S.p. HiFi Cas9 nuclease (Integrated DNA Technologies) and 1.75 µg (50 pmol) of single-guide RNA (sgRNA) diluted with 20 µl of OptiMEM (Thermo Fisher Scientific) supplemented with 7.25 mM ATP and 11.8 mM $MgCl_2$, then they were incubated at room temperature for 10 min. During that time, cells were collected with Accutase (Innovative Cell Technologies), then 400,000 cells were suspended with the prepared solution and electropration was performed using a 16-well Nucleocuvette Strip with 4D Nucleofector system (Lonza) using CA137 on P3 primary cell electroporation code. Immediately after electroporation,

cells were transferred into one well of a matrigel-coated six-well plate containing mTeSR medium with 10 µM Y-27632 and cultured for 24 h. The medium was then changed, and Y-27632 was removed after 48 h of electroporation. Single cell cloning was started after four days of electroporation. Genotype was determined by PCR with the primer set Fwd, TTTAACTTGGTACCAGGGAATTGGA; Rev, TCATCCTTCTTATCAGCACTCTCAC, followed by gel extraction and Sanger sequencing performed by MCLab using the primer gtcgccagtcacttaagctgag. TIDE analysis (https://tide.deskgen.com/) was performed with obtained chromatgrams to judge the genotypes of each clone. Synthetic sgRNA was purchased from Synthego with chemically modified nucleotides at the three terminal positions at both the 5′ and 3′ ends. Modified nucleotide contained 2′-*O*-methyl 3′-phosphorothioate. The genomic sgRNA target sequence was gggcccacacgggagcggag.

Off-target candidates were predicted using the COSMID46 tool (https://crispr.bme.gatech.edu). Integrity was confirmed by Sanger sequencing at the top three off-target candidates (Chr6: 138404602–138404624 GCGCCGACTCGGGAGCGGAGGGG, Chr3: 52534180–52534202 GGGCGGACCCGGGAGCGGAGAGG, Chr3: 49902616–49902638 GGGCACCCACTGGAGCGGAGTGG).

**hiPS cell genotyping.** The Illumina genome-wide SNP microarray 'GSAMD-24v2-0' (with 759,993 probes) was used to genotype the samples. Probe level log R ratio (LRR) and B-allele frequency (BAF) values were created using Illumina GenomeStudio software. PennCNV (1.0.4) detect_cnv was used to create a list of putative copy-number variation (CNV) calls in each sample based on the LRR and BAF profiles of contiguous SNPs. PennCNV clean_cnv was then used to merge potentially fragmented neighboring CNV calls. PennCNV visualize_cnv was run to review the underlying LRR and BAF profiles of CNV calls of at least 100 kb genome-wide.

**High-performance liquid chromatography measurements.** Media from neuronal cultures at day 43 of differentiation was collected and stored with 7 M $HClO_4$ (7 µl for 0.5 ml of medium) at −80 °C until further analysis. NE, DA, glutamate (GLUT) and GABA levels in the samples were determined by HPLC with electrochemical detection. The medium was centrifuged and the supernatant was filtered. For catecholamine measurements, the filtered supernatant was injected into the column. The HPLC mobile phase (0.1 M sodium phosphate buffer, 0.13 mM EDTA, 2.3 mM 1-octanesulfonic acid, 20% MeOH, pH 6.0) was pumped through a chromatography column (SC-5ODS, Eicom) and a 50 µl sample loop at a flow rate of 0.23 ml $min^{-1}$. A graphite electrode (WE-3G, Eicom) set at a potential of 450 mV was used for electrochemical detection. For the amino acid measures, the filtered supernatant was diluted 100 times with 10% MeOH. A 60-µl volume of each sample was derivatized with 20 µl of *o*-phthalaldehyde solution for 2.5 min at room temperature and then injected into the column. The mobile phase was a 0.1 M sodium phosphate buffer, pH 6.0, 5 mg $l^{-1}$ EDTA, with 30% MeOH, which was pumped at a flow rate of 0.23 ml $min^{-1}$. The graphite electrode was set at +600 mV against an Ag–AgCl reference electrode. Quantification was achieved with a PowerChrom analysis system (ADInstruments) using external standards (Sigma). Experiments were conducted blind to the disease status of the samples. The concentration was calculated by comparing the HPLC peak of each neurotransmitter in samples with the peak area of known concentrations of the standards analyzed on the same day. The levels of neurotransmitters were normalized to the total number of cells per well.

**Calcium imaging.** Calcium imaging was performed as previously described[23]. Experiments in the initial calcium phenotyping assay were conducted blind to disease status. Cells used in calcium imaging experiments were from dissociated hCSs plated on coverslips (15 mm, Warner Instruments, 640713). Briefly, cells were loaded with 1 µM Fura-2 acetoxymethyl ester (Invitrogen) for 30 min at 37 °C in NM medium, washed with NM medium for 10 min and then transferred to a perfusion chamber (RC-20, Warner instruments) in low-potassium Tyrode's solution (2 mM KCl: 129 mM NaCl, 2 mM $CaCl_2$, 1 mM $MgCl_2$, 30 mM glucose, 25 mM HEPES 0.1%, BSA, pH 7.4) on the stage of an inverted fluorescence microscope (Eclipse TE2000U; Nikon). After imaging for 2 min (or 1 min with a 2-min baseline treatment of drug), high-potassium Tyrode's solution (high-KCl) (67 mM KCl: 67 mM NaCl, 2 mM $CaCl_2$, 1 mM $MgCl_2$, 30 mM glucose and 25 mM HEPES, 0.1% and BSA, pH 7.4) was applied. Imaging was performed at room temperature (~25 °C) on an epifluorescence microscope equipped with an excitation filter wheel and an automated stage. Openlab software (PerkinElmer) and IGOR Pro (version 5.1, WaveMetrics) were used to collect and quantify time-lapse excitation ratio images, as previously described[63]. JMP (v15, SAS Institute) was used for the mixed-model analysis and Prism (v8.4, GraphPad) was used for all other statistical analyses. Only cells that had a response higher than 0.1 (340 nm/380 nm) were included in the analysis (no threshold was applied for cells analyzed in nimodipine experiments). For pharmacology experiments, the following concentrations were used: TTX (1 µM), sulpiride (10 µM), raclopride (10 µM), APV (20 µM) and NBQX (20 µM).

**Patch-clamp electrophysiology in hCS neurons.** For patch-clamp recordings, cells were identified by the presence of a fluorescent reporter (Syn1::YFP$^+$) using an upright 'slicescope' microscope (Scientifica) and OCULAR (Qimaging) software. Experiments were conducted blind to the disease status of the samples. Neurons from dissociated hCSs, which were cultured for at least five days, were bathed in an external solution of BrainPhys neuronal medium (STEMCELL Technologies, 05790). Recording electrodes of borosilicate glass had a resistance of 7–15 MΩ when filled with an internal solution containing the following: 145 mM K gluconate, 0.1 mM $CaCl_2$, 2.5 mM $MgCl_2$, 10 mM HEPES, 0.2 mM EGTA and 4 mM Na-phosphocreatine. Command voltage protocols were generated and extracellular and whole-cell data were collected using a 1550A digitizer (Molecular Devices) and a 700B patch-clamp amplifier (Molecular Devices) and were acquired with pClamp 10.6 software (Molecular Devices). Data were low-pass-filtered at 2–10 kHz and digitized at 20 kHz. Care was taken to keep the membrane access resistance as low as possible (usually 5–8 MΩ and always less than 13 MΩ). Capacitive currents were reduced before break-in using the amplifier circuitry. Data averaging, digital subtraction of null traces and AP detection were carried out with MATLAB (MathWorks) and Clampfit (Molecular Devices). Data were fitted and plotted using MATLAB (MathWorks) and Origin (OriginLab).

To determine if neurons are spontaneously firing, we analyzed current traces obtained in the cell-attached configuration at 0 mV holding potential. A neuron was considered spontaneously active if an extracellular spike was detected within a 2-min recording window. Spikes were detected using a threshold of three standard deviations from the current mean. To minimize noise artefacts, traces were low-pass-filtered (500 Hz, −3 dB, low-pass Gaussian filter) before analysis.

For spike train recordings in whole-cell mode, neurons were held near −70 mV with steady current injections and 1-s current injections were given at 10-s intervals to elicit spike trains. Recordings were corrected for an estimated −15-mV liquid junction potential.

For recordings of calcium channel currents, an internal solution was used that contained 110 mM $CsMethylSO_3$, 30 mM TEA-Cl, 10 mM EGTA, 4 mM MgATP, 0.3 mM $Na_2GTP$, 10 mM HEPES, 5 mM QX314-Cl, pH 7.2 with CsOH, 290 mOsm. The external solution contained 114 mM NaCl, 25 mM TEA-Cl, 3 mM KCl, 2 mM $MgCl_2$, 4 mM $BaCl_2$, 4 mM 4-aminopyridine, 10 mM HEPES, 20 mM glucose, pH 7.4 with NaOH, 300 mOsm. In voltage-clamp recordings, currents were leak subtracted using a –P/4 protocol. Between sweeps, cells were held at −70 mV.

For RMP recordings, the following drug applications were used: sulpiride (10 µM), raclopride (10 µM) and olanzapine (10 µM).

**Simultaneous patch clamping and calcium imaging.** Simultaneous patch clamping and calcium imaging was performed using Fura-2 pentapotassium salt (Thermo Fisher F1200) on dissociated hCS neurons, alternately excited with two high-intensity light-emitting diode (LED) devices (340 and 385 nm; Prizmatix). Experiments were conducted blind to the disease status of the samples. To minimize crosstalk between the 340- and 385-nm LEDs, two band-pass CHROMA excitation (ET) filters, ET340x and ET340x (Chroma), respectively, were situated immediately after the LEDs. Emission was collected with the rest of the 79001-filter set (dichroic = 400 nm, emission = 510 nm). Changes in fluorescence were acquired using Retiga a ELECTRO charge-coupled device (Teledyne Q-imaging). Images were acquired at one frame per second for each wavelength. Both the camera frame rate and LED timing were trigger-controlled by an Arduino system (arduino.cc) using custom software. To improve the signal-to-noise ratio of the traces, several trials were typically averaged.

**Electrophysiology in 2D neurons.** Whole-cell patch-clamp recordings were conducted in current-clamp or voltage-clamp mode, visualizing neurons using a Nikon Eclipse FN1 upright microscope and amplifying signals via a Multiclamp 700B system (Axon Instruments). Experiments were conducted blind to the disease status of the samples in neurons at 50–70 days of differentiation in vitro. For recordings in current-clamp mode, pipettes (3–5 MΩ resistance) were filled with an internal solution consisting of 120 mM potassium gluconate, 20 mM KCl, 4 mM NaCl, 4 mM $Mg_2ATP$, 0.3 mM NaGTP, 10 mM $Na_2$-phosphocreatine, 0.5 mM EGTA, 10 mM HEPES, pH 7.25 with KOH, 290 mOsm. Neurons (Syn1::YFP$^+$) cultured on glass coverslips were bathed in an external solution containing 140 mM NaCl, 2.5 mM KCl, 1 mM $NaH_2PO_4$, 10 mM HEPES, 2.5 mM $CaCl_2$, 2 mM $MgCl_2$, 20 mM glucose pH 7.4 with NaOH, 300 mOsm.

For recordings of calcium channel currents, an internal solution containing 110 mM $CsMethylSO_3$, 30 mM TEA-Cl, 10 mM EGTA, 4 mM MgATP, 0.3 mM $Na_2GTP$, 10 mM HEPES, 5 mM QX314-Cl, pH 7.2 with CsOH, 290 mOsm was used. The external solution contained 90 mM NaCl, 25 mM TEA-Cl, 3 mM KCl, 2 mM $MgCl_2$, 20 mM $BaCl_2$, 4 mM 4-aminopyridine, 10 mM HEPES, 20 mM glucose, pH 7.4 with NaOH, 300 mOsm. For measuring calcium currents, 20 mM $CaCl_2$ was substituted for $BaCl_2$.

**RNA-seq processing.** Libraries were prepared using TruSeq stranded RNA RiboZero Gold (Illumina) from rRNA depleted (RiboZero Gold, Illumina). 100-bp paired end reads were sequenced using an Illumina HiSeq 4000. Reads were mapped to hg38 with Gencode v25 annotation using STAR (v2.5.2b)[64]. Gene expression was quantified using rsem (v1.3.0)[65]. Genes with less than 10 reads in over 50% of samples per time point were discarded leaving 17,071 genes in the analysis. Outlying samples were identified by having a standardized

sample network connectivity Z scores smaller than −2, and were removed[66]. Picard sequencing metrics (http://broadinstitute.github.io/picard/, v2.5.0) were summarized using the first 20 principal components (seqPCs). These seqPCs were then included in the model to control for technical variation in the RNA sequencing. Batch effect were accounted for by either including batch as a covariate in the linear model (allowing for correct estimation of degrees of freedom) or by Combat function form the sva package in R (for PCA and correlation analysis)[67].

Sample identity was verified using the identity by descent (IBD) algorithm from PLINK (1.09). IBD was calculated for each sample based on genotypes derived from RNA-seq analysis and a threshold of PI_HAT < 0.8 was set. Additionally, for each hiPS cell line, the sex was verified by detection of genes expressed by the Y chromosome. To account for differences in gene expression caused by common variation associated with genetic ancestry, SNPs were called from the aligned reads using the GATK (v3.3) Haplotype caller[68]. The results were then converted to plink format (v1.08) and filtered for quality (<5% missing values, minor allele frequency < 0.05, and Hardy–Weinberg equilibrium < $1 \times 10^{-6}$)[69]. Multidimensional scaling (MDS) was calculated on the resulting high-quality SNPs which were combined with HapMap3.3 (hg38) to estimate genetic ancestry. Variance partitioning was performed using the variancePartition package (v1.14.1) with default parameters in R.

**Batch effects.** Batches were balanced for control and 22q11DS lines. However, within one of the batches the cases and controls were split and pooled separately and sequenced on different flow cells. To account for this, samples from both control and 22q11DS lines were resequenced at one time point (day 75). These samples were then included in the analysis while using a random variable to account for them being sequenced twice. Additionally, to estimate the effect of this splitting of samples on the DEG at each time point, a linear model was run measuring the interaction between the spilt batch and the presence of the 22q11.2 deletion on the DEGs. A significant interaction term would indicate that this batch had a significantly different effect on expression than the other batches. No significant interaction or skewness in the distribution was observed. Moreover, in a case where the splitting had a large effect on observed gene expression levels, the expected distribution of the effect size of the interaction term should be right skewed. This expectation for a right-skewed distribution results from the assumption that the splitting created a larger (positive) difference between the cases and controls, which should lead to a right-shifted or skewed distribution.

**Differential expression.** Differential expression was performed using conditional quantile-normalized[70] expression levels, which account for gene length, library size and G/C content. A mixed linear model was used to account for multiple samples coming from the same individual, hiPS cell line and differentiation, as well as to account for samples that were sequenced more than once. Fixed covariates that were included were differentiation day, sex, batch, the first two PCs calculated for genetic ancestry and 20 sequencings PCs (SeqPCs). The model was implemented using the lme function from the nlme package (v3.1.143) in R. Contrasts were used to compare between cases and controls within each time point using the glht function from the multcomp package (v1.4.12) in R. Genes with FDR < 0.05 were considered to be differentially expressed. Data were plotted using the tidyverse (v1.2.10) and ggplot2 (v3.2.1) packages in R.

**Gene set enrichment analysis.** GSEA was performed using the fgsea package (v1.10.1)[71] in R on all genes ranked by log$_2$ fold change. The parameters used were 1,000,000 permutations, a minimal set size of 30 and a maximal set size of 500. Gene ontology gene sets (v7.0) were downloaded from http://software.broadinstitute.org/gsea/msigdb/. Gene sets with FDR < 0.05 were considered to be significant.

**Genome-wide association study enrichment.** DEGs were tested for GWAS enrichment from ASD[32], SCZ[33] and ADHD[34] studies. SNPs were assigned to a gene if they were within 10 kb of a gene and were used. SNP heritability was estimated using a stratified LDscore (v1.0.0) regression[72]. Enrichment was then calculated as the proportion of SNP heritability accounted for by the DEG divided by the proportion of total SNPs within the DEG. Significance was tested using a jackknife method, followed by FDR correction. Enrichments with FDR < 0.05 were considered significant.

**Power analysis.** Power analysis was performed using the PROPER package (v1.10.0)[73] in R. The analysis was run using the first batch of data and used 17,000 genes, with an estimated 5% of genes being differentially expressed. The simulation was run 100 times using the edgeR differential expression method[74] with 5, 10, 15, 20 and 30 samples. Power was calculated for log fold changes ranging from 0.25 to 1.5, which is equivalent to changes of ~18% to ~180% in expression level.

**Single cell gene expression.** Dissociations were carried out as previously described[22]. Dissociated cells were resuspended in ice-cold PBS containing 0.02% BSA and loaded onto a Chromium Single cell 3′ chip (with an estimated recovery of 10,000 cells per channel) to generate gel beads in emulsion (GEMs). scRNA-seq libraries were prepared with the Chromium Single cell 3′ GEM, Library & Gel Bead Kit v2 (10x Genomics, PN: 120237). Libraries from different samples were pooled and sequenced by Admera Health on a NovaSeq S4 (Illumina) using 150 × 2 chemistry. Sample demultiplexing, barcode processing and unique molecular identifiers counting was performed using the Cell Ranger software suite (v3.0 with default settings). Reads were then aligned to the human reference genome (GRCh38), filtered, and counted using the Cell Ranger count pipeline. Processed samples with a cellular yield of more than 200% of the estimated recovery (10,000 cells) or less than 70% fraction reads in cells were excluded. Expression matrices for the remaining samples were processed using the R (v3.6.1) package Seurat (v3.0) from the Satija Lab[75]. We excluded genes that were not expressed in at least three cells. We excluded cells with fewer than 500 detected genes, as well as those with a proportion of mitochondrial reads higher than 30%. Gene expression was then normalized using a global-scaling normalization method (normalization.method='LogNormalize', scale.factor = 10,000), and the 2,000 most variable genes were then selected (selection.method='versust'). Individual samples were aggregated into one Seurat object by implementing FindIntegrationAnchors and IntegrateData with default settings (as recommended by Seurat). Aggregated gene expression was then scaled (mean = 0 and variance = 1, for each gene, as recommended by Seurat) before PCA. The top 30 PCs were utilized to perform a *t*-SNE projection, implemented with the RunTSNE function with default settings, and to do the clustering with a resolution of 0.4, implemented using the FindNeighbors and FindClusters functions. We identified clusters based on differential expression of known markers, identified using the FindAllMarkers function with default settings[22]. In some cases, using expression of known markers, we grouped together clusters that were originally separate based on the Seurat clustering; the 'Glutamatergic neurons', 'Radial glia', 'Astroglia' and 'M cell cycle' clusters were composed of 2–7 clusters. R packages ggplot (v3.2.1) and pheatmap (v1.0.12) were utilized to create figures.

**Reporting Summary.** Further information on research design is available in the Nature Research Reporting Summary linked to this Article.

## Data availability

Gene expression data are available in the Gene Expression Omnibus (GEO) under accession nos. GSE142041 and GSE145122. The data that support the findings of this study are available on request from the corresponding author.

## References


61. Yazawa, M. et al. Using induced pluripotent stem cells to investigate cardiac phenotypes in Timothy syndrome. *Nature* **471**, 230–234 (2011).
62. Birey, F. et al. Assembly of functionally integrated human forebrain spheroids. *Nature* **545**, 54–59 (2017).
63. Barreto-Chang, O. L. & Dolmetsch, R. E. Calcium imaging of cortical neurons using Fura-2 AM. *J. Vis. Exp.* **9**, 1067 (2009).
64. Dobin, A. et al. STAR: ultrafast universal RNA-seq aligner. *Bioinformatics* **29**, 15–21 (2013).
65. Li, B. & Dewey, C. N. RSEM: accurate transcript quantification from RNA-Seq data with or without a reference genome. *BMC Bioinformatics* **12**, 323 (2011).
66. Oldham, M. C., Langfelder, P. & Horvath, S. Network methods for describing sample relationships in genomic datasets: application to Huntington's disease. *BMC Syst. Biol.* **6**, 63 (2012).
67. Johnson, W. E., Li, C. & Rabinovic, A. Adjusting batch effects in microarray expression data using empirical Bayes methods. *Biostatistics* **8**, 118–127 (2007).
68. McKenna, A. et al. The genome analysis Toolkit: a MapReduce framework for analyzing next-generation DNA sequencing data. *Genome Res.* **20**, 1297–1303 (2010).
69. Purcell, S. et al. PLINK: a tool set for whole-genome association and population-based linkage analyses. *Am. J. Hum. Genet.* **81**, 559–575 (2007).
70. Hansen, K. D., Irizarry, R. A. & Wu, Z. Removing technical variability in RNA-seq data using conditional quantile normalization. *Biostatistics* **13**, 204–216 (2012).
71. Korotkevich, G., Sukhov, V. & Sergushichev, A. Fast gene set enrichment analysis. Preprint at *bioRxiv* 060012 https://www.biorxiv.org/content/10.1101/060012v2 (2019).
72. Finucane, H. K. et al. Partitioning heritability by functional annotation using genome-wide association summary statistics. *Nat. Genet.* **47**, 1228–1235 (2015).
73. Wu, H., Wang, C. & Wu, Z. PROPER: comprehensive power evaluation for differential expression using RNA-seq. *Bioinformatics* **31**, 233–241 (2015).
74. Robinson, M. D., McCarthy, D. J. & Smyth, G. K. edgeR: a Bioconductor package for differential expression analysis of digital gene expression data. *Bioinformatics* **26**, 139–140 (2010).
75. Butler, A., Hoffman, P., Smibert, P., Papalexi, E. & Satija, R. Integrating single-cell transcriptomic data across different conditions, technologies and species. *Nat. Biotechnol.* **36**, 411–420 (2018).

## Acknowledgements

We thank the families who participated in this study. We acknowledge J. Andersen, J. Y. Park and all members of the Pasca Laboratory for support, as well as A. Trevino, A. E. Urban and H. Gai at Stanford University for scientific discussions and technical support. This work was supported by the US National Institutes of Health (NIH) BRAINS Award (MH107800), the NARSAD Young Investigator Award (Behavioral and Brain Foundation), the MQ Fellow Award, the NYSCF Robertson Stem Cell Investigator Award, the CZI Ben Barres Investigator Award, the Stanford Human Brain Organogenesis Program and the Brain Rejuvenation Project, Uytengsu Research Funds, the Kwan Research Fund and the California Institute of Regenerative Medicine (CIRM) (to S.P.P.); NIH R01MH100900 (J.F.H., C.E.B., R.O., J.A.B., D.H.G. and S.P.P.) and R01MH100900-S1 (J.F.H. and S.P.P.); NIMH R01 MH085953 and R01 MH085953-08:S1 (CEB); NIMH 5R37 MH060233 and 5R01 MH094714 (D.H.G.); National Research Foundation of Korea grant no. NRF-2019R1A2C3002354 (to C.H.K); the Lucile Packard Foundation for Children's Health (anonymous gift for 22q11DS research; M.H.P.); the National Institute of Mental Health (J.L.R.); Stanford Graduate Fellowship (SGF) and National Science Foundation (NSF) Fellowship (T.A.K.); the Stanford Dean's Fellowship, the Feldman Gift Fund and the Maternal and Child Health Research Institute (MCHRI) Fellowship (O.R.); the Autism Science Foundation (ASF) and the Brain and Behavior Research Foundation (BBRF) Young Investigator award (A.G.); the HHMI Fellowship (A.K.K.); the Stanford Bio-X Undergraduate Fellowship (J.M.S.); the DGIST R&D Program of the Korean Ministry of Science and ICT & Future Planning, 14-BD-16 (C.-H.K.).

## Author contributions

T.A.K., O.R. and S.P.P. designed experiments. T.A.K. and S.P.P. wrote the manuscript with input from all authors. T.A.K. and S.-J.Y. performed the differentiation experiments and characterization of hCSs. S.-J.Y., M.Y. and S.P.P. generated, validated and differentiated hiPS cell lines. T.A.K., O.R. and S.P.P. conducted and analyzed the calcium imaging experiments. O.R., M.-Y.L., C.G., Y.S. and J.R.H. conducted and analyzed electrophysiological experiments. A.K.K., C.H.K., S.P.P. and R.E.D. performed and characterized 2D cortical neural cultures and established assays. A.G., Y.T. and D.H.G. analyzed the bulk RNA sequencing. T.A.K., J.M.S. and N.D.A. carried out single-cell RNA-seq experiments and analysis. K.I and M.H.P. generated the *DGCR8*$^{+/-}$ hiPS cell line. N.S. and S.N. performed the HPLC experiments. J.L.R., J.A.B., R.O., C.E.B., J.F.H. and L.K. recruited and collected the cohort of subjects. S.P.P. supervised all aspects of the work.

## Competing interests

Stanford University was granted a patent that covers the generation of region-specific brain organoids (US patent 15/158,408). Y.S., C.G. and R.E.D. were employees of Novartis Institute of Biomedical Institutes for part of the duration of this study.

## Additional information

**Extended data** is available for this paper at https://doi.org/10.1038/s41591-020-1043-9.

**Supplementary information** is available for this paper at https://doi.org/10.1038/s41591-020-1043-9.

**Correspondence and requests for materials** should be addressed to S.P.P.

**Peer review information** Kate Gao and Joao Monteiro were the primary editors on this article and managed its editorial process and peer review in collaboration with the rest of the editorial team.

**Reprints and permissions information** is available at www.nature.com/reprints.

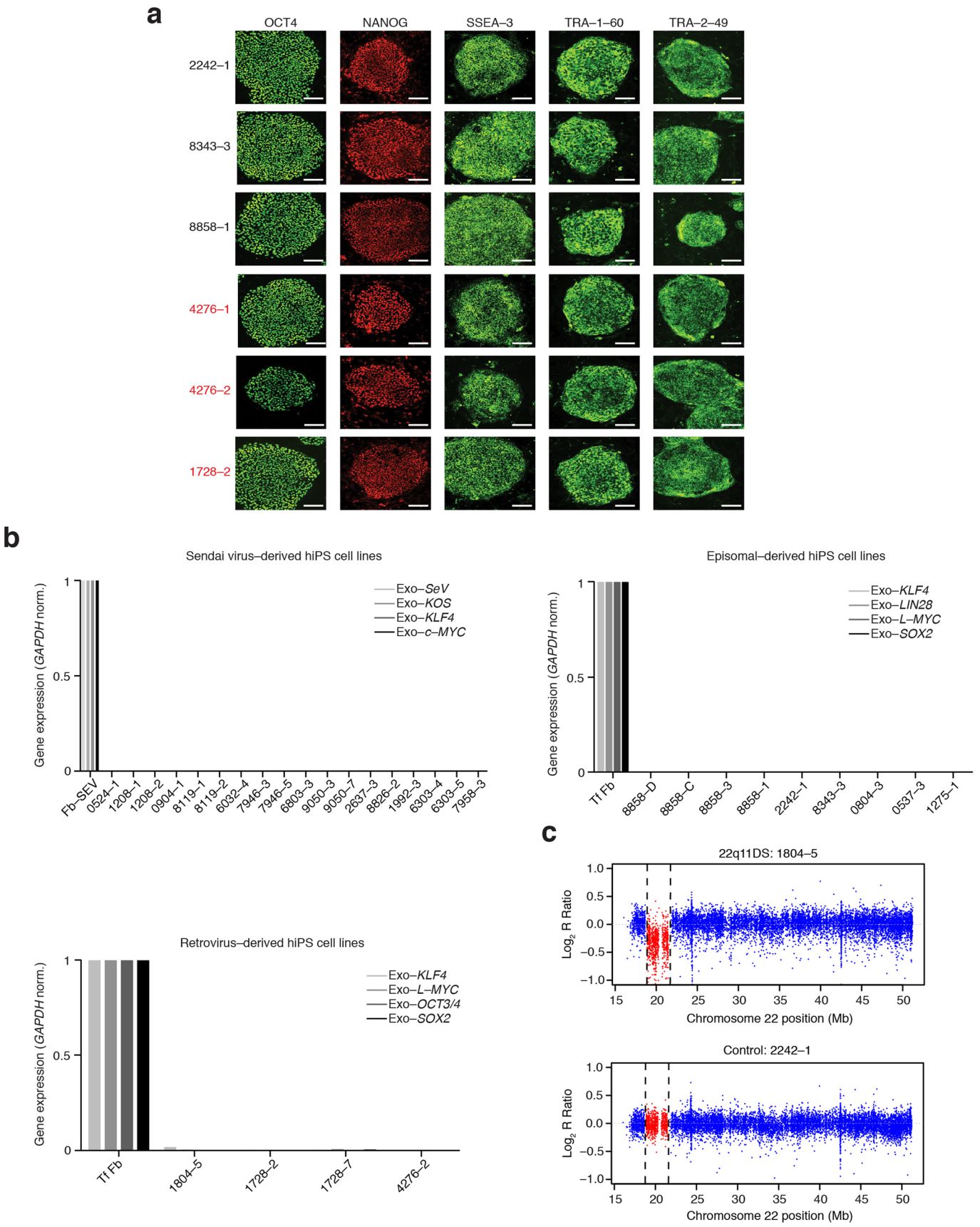


**Extended Data Fig. 1 | See next page for caption.**

**Extended Data Fig. 1 | Characterization of hiPS cell lines derived from control and 22q11DS subjects. a**, Immunocytochemistry for pluripotency markers with antibodies against OCT4, NANOG, SSEA-3, TRA-1-60, TRA-2-49. Images from one experiment. Selected hiPS cell lines are shown, black indicates control lines and red indicates 22q11DS lines. Scale bar= 200 μm. **b**, Expression of endogenous and silencing of exogenous pluripotency genes (qPCRs) in Sendai, episomal or retroviral based reprogramming into hiPS cells. Tf FB or FB-SeV indicate fibroblasts transduced with the reprogramming vectors. Mean ± SEM. (**c**) Example of genome-wide SNP microarray genotyping of a control and a 22q11DS hiPS cell line. For further details on deletion coordinates for all 22q11DS subjects, see Supplementary Table 4.

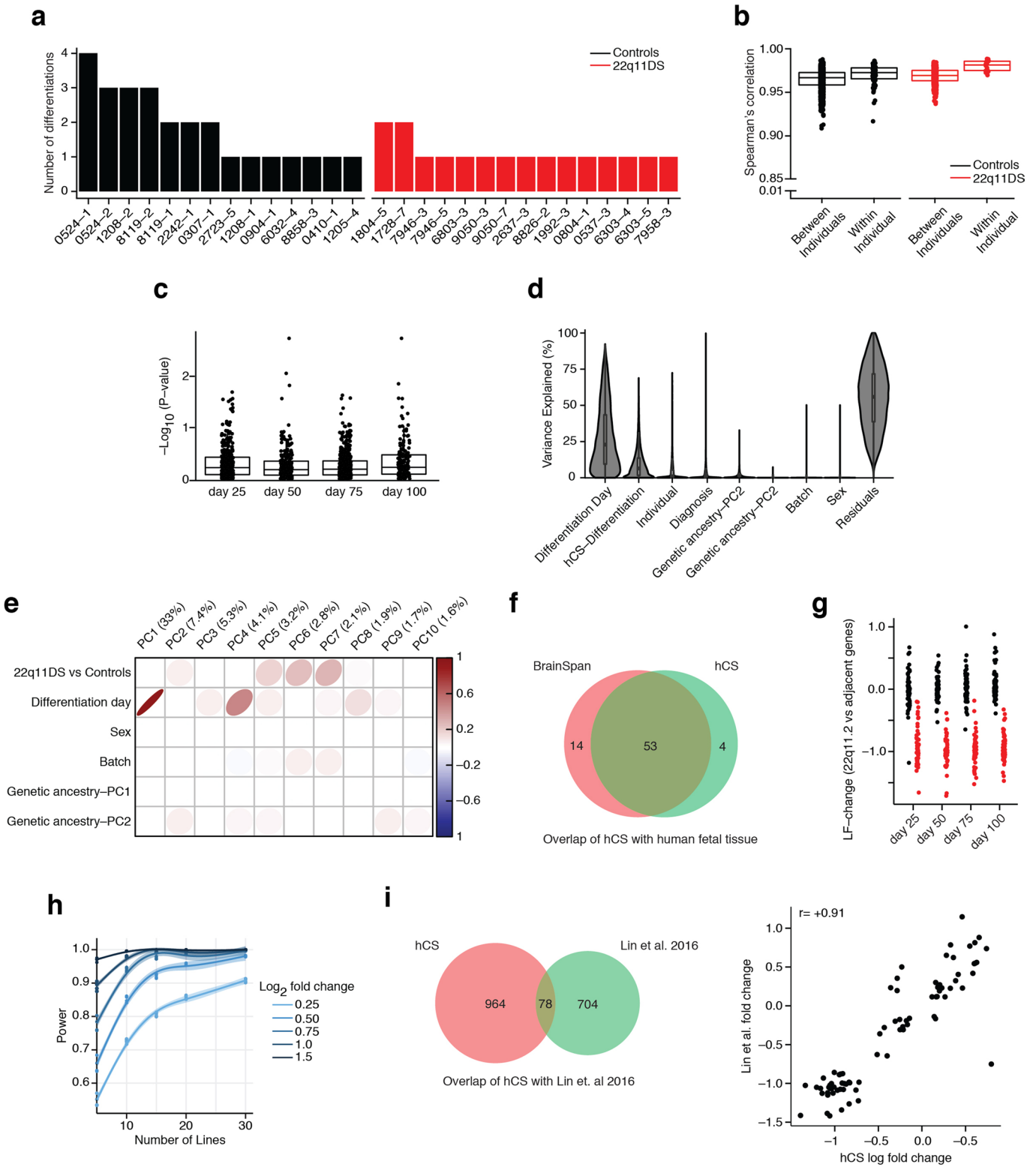


**Extended Data Fig. 2 | See next page for caption.**

**Extended Data Fig. 2 | RNA-sequencing analysis of hCS in 22q11DS. a**, Number of differentiations into hCS from each hiPS cell lines; controls (black, $n = 26$) and 22q11DS (red, $n = 17$). Height of the bar shows the number of independent differentiation experiments. **b**, Spearman's correlation coefficients (mean ~ 0.97) between differentiations of the same cell line (within individuals) or between different hiPS cell lines (between individuals) (two-sided Wilcoxon–Mann–Whitney test, $P < 0.05$, controls, $n = 104$ samples from 14 control hiPS cell lines derived from 11 subjects; 22q11DS, $n = 71$ samples derived from 15 patient hiPS cell lines derived from 12 subjects). **c**, No significant interaction between the split batch (see Methods) and presence of a 22q11.2 deletion in DEGs. Values are -log of the uncorrected *P* values (controls, $n = 25$ samples from the split batch and $n = 79$ from the other batches from 14 control hiPS cell lines derived from 11 subjects; 22q11DS, $n = 33$ samples from the split batch and $n = 38$ from the other batches from 15 patient hiPS cell lines derived from 12 subjects). **d**, Violin plots of the percent of variance explained by each of the covariates on the x-axis for each gene. **e**, Association of the expression principal components (PC) with biological and technical covariates. **f**, Overlap of genes in the 22q11.2 deletion locus that are expressed in vivo (BrainSpan dataset, red) and in hCS (green). **g**, $Log_2$ fold change in 22q11DS neurons of genes in the 22q11.2 locus (red) compared to genes adjacent to the 22q11.2 deletion locus (black). **h**, Power calculation based on the samples in the first batch of sequencing. The sample size in this study (20 differentiations) leads to a power of 0.85 to detect a $log_2$ fold change of 0.25 (~18% change in expression). **i**, Overlap of DEG in 22q11DS hCS and DEG reported in Lin et al., 2016 (left) (using $P < 0.05$ across all datasets). Right, correlation between log fold-changes overlapping DE (Spearman's $R = 0.91$, $P = 1.11e^{-30}$). For (b, d, e, f): Controls, $n = 104$ samples from 14 control hiPS cell lines derived from 11 subjects; 22q11DS, $n = 71$ samples derived from 15 patient hiPS cell lines derived from 12 subjects. For (b, c, e): Center shows median, box shows 25th to 75th percentile, lower whisker shows smallest observation great than or equal to lower hinger -1.5x interquartile range, upper whisker shows largest observation less than or equal to upper hinger +1.5x interquartile range.

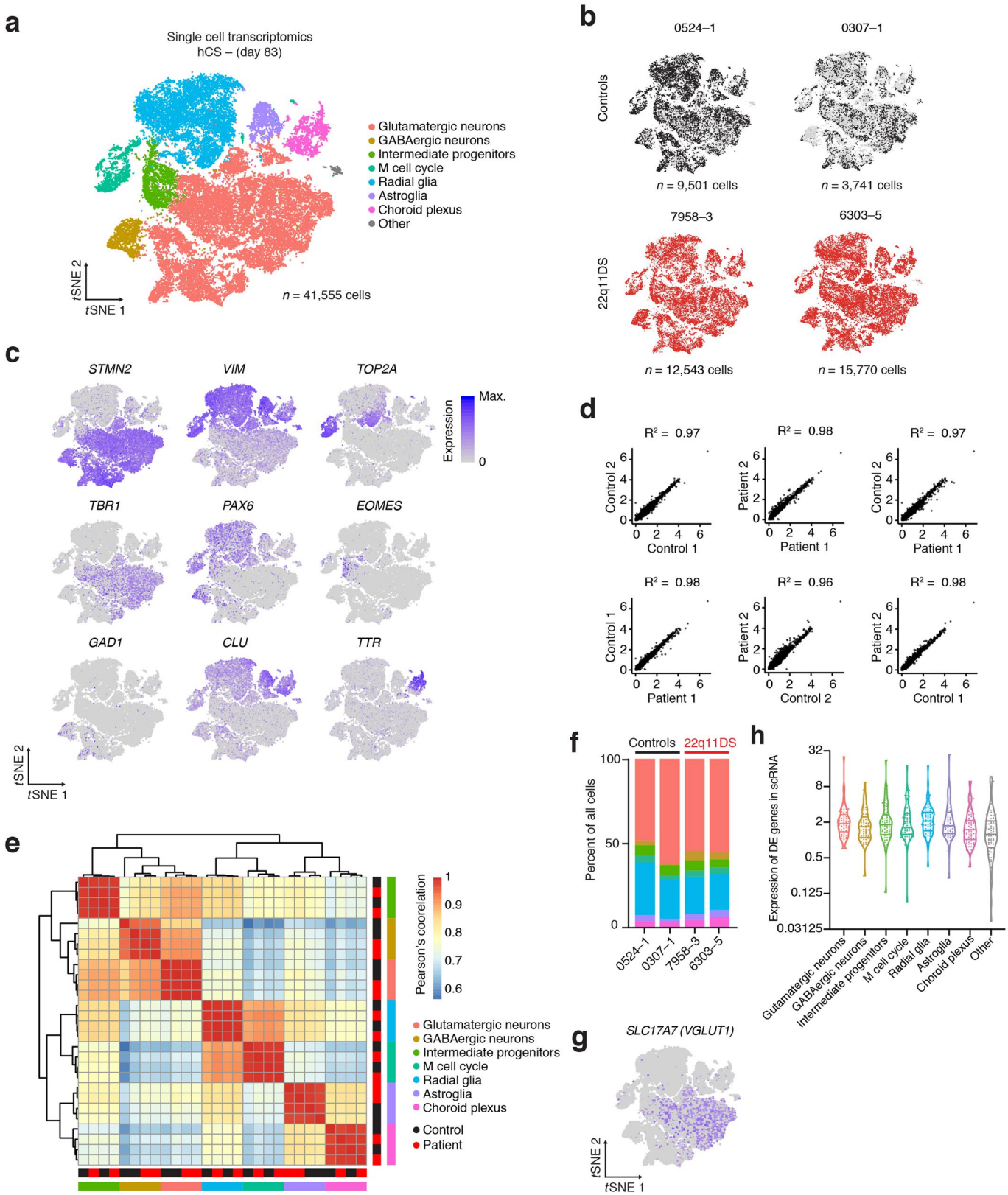


**Extended Data Fig. 3 | Single cell transcriptional profiling of hCS derived from 22q11DS and control hiPS cell lines. a**, Droplet-based single-cell transcriptomics (10x Genomics Chromium) in four hiPS cell lines ($n = 41,555$ cells from two control hiPS cell lines derived from two subjects, and two patient hiPS cell lines derived from two subjects). **b**, Control and 22q11DS samples shown by line (two control lines and two 22q11DS lines). **c**, Gene expression, shown by the presence of clusters neuronal clusters, of the aggregated data of two control lines and two 22q11DS lines. **d**, Pearson's correlation of all genes across all four lines (two control lines and two 22q11DS lines, $R^2 > 0.96$). **e**, Gene expression across group and cluster (two control lines and two 22q11DS lines). **f**, Proportion of cells in each cluster across lines (two control lines and two 22q11DS lines). **g**, Expression across all lines (two control lines and two 22q11DS lines). **h**, Expression across cell clusters in single cell gene expression of DEG identified in the bulk RNA-seq (at day 75).

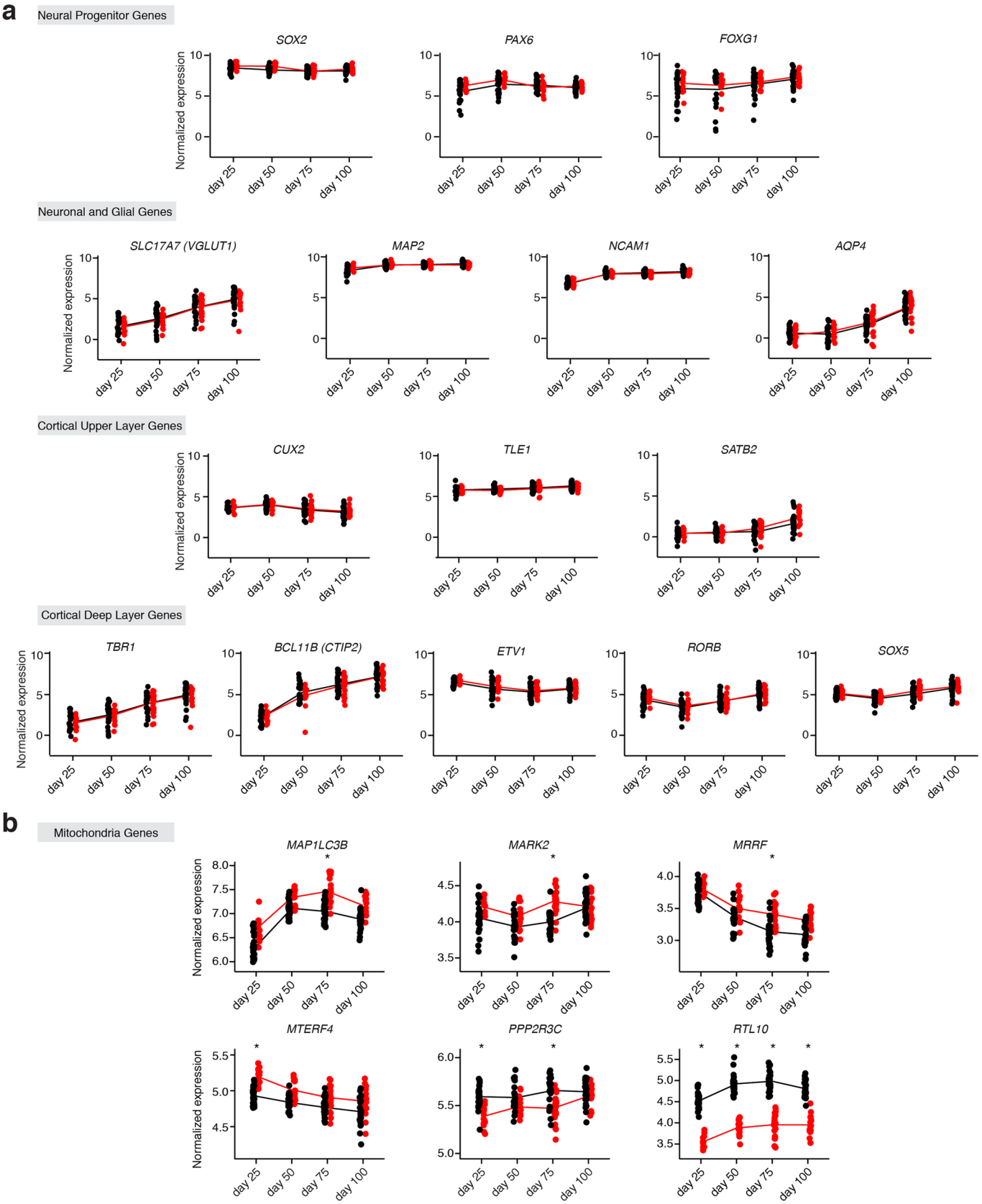


**Extended Data Fig. 4 | See next page for caption.**

**Extended Data Fig. 4 | Temporal trajectory of gene expression (RNA-seq) for selected cortical markers and mitochondrial genes in intact hCS.** **a**, Selected cortical marker trajectories in 22q11DS (red) and control lines (black) in whole hCS. Controls, $n = 26$ (day 25 hCS), $n = 25$ (day 50 hCS), $n = 28$ (day 75 hCS), and $n = 25$ (day 100 hCS) samples from 14 control hiPS cell lines derived from 11 subjects; 22q11DS, $n = 14$ (day 25 hCS), $n = 16$ (day 50 hCS), $n = 24$ (day 75 hCS), and $n = 17$ (day 100 hCS) samples derived from 15 patient hiPS cell lines derived from 12 subjects. **b**, Selected mitochondria genes trajectories in 22q11DS (red) and control lines (black) in hCS. Asterisks indicate differential expression at the specified timepoints between control and 22q11DS lines (FDR< 0.05). Controls, $n = 26$ (day 25 hCS), $n = 25$ (day 50 hCS), $n = 28$ (day 75 hCS), and $n = 25$ (day 100 hCS) samples from 14 control hiPS cell lines derived from 11 subjects; 22q11DS, $n = 14$ (day 25 hCS), $n = 16$ (day 50 hCS), $n = 24$ (day 75 hCS), and $n =17$ (day 100 hCS) samples derived from 15 patient hiPS cell lines derived from 12 subjects.

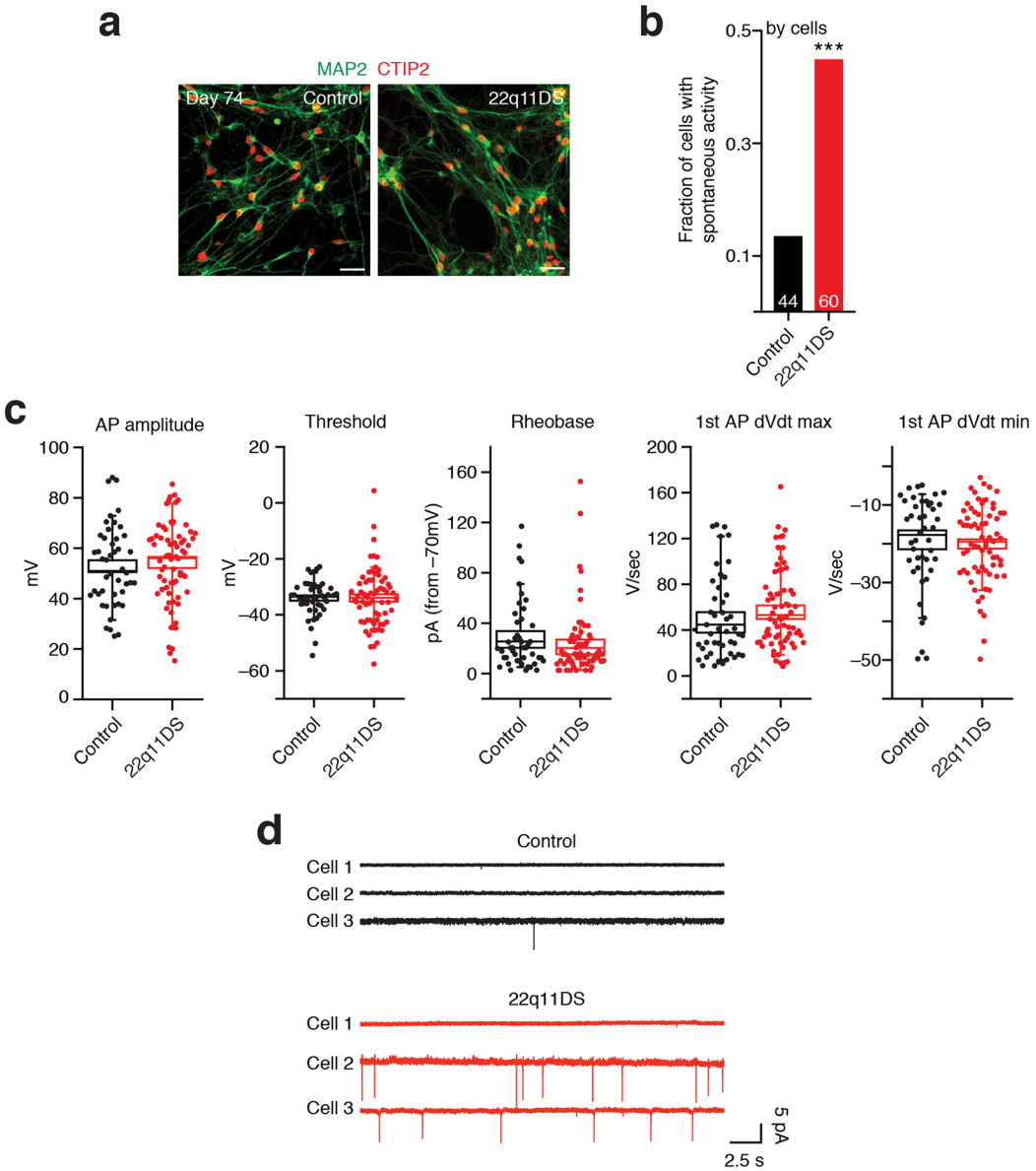


**Extended Data Fig. 5 | Electrophysiological characterization of hCS-derived neurons in 22q11DS. a**, Immunostaining of hCS-plated neuronal cultures with anti-CTIP2 and anti-MAP2 antibodies. Representative images from over 3 independent experiments with similar results. Scale bar = 50 μm. **b**, Proportion of cells with spontaneous action potentials (controls, $n = 44$ cells derived from 6 control hiPS cell lines derived from 6 subjects; 22q11DS, $n = 60$ cells derived from 5 patient hiPS cell lines derived from 4 subjects; chi-square test for proportion of cells, $\chi^2$=11.52, ***$P = 0.0006$). **c**, Comparison of action potential properties (controls, $n = 46$ cells derived from 6 control hiPS cell lines; 22q11DS, $n = 66$ cells derived from 4 patient hiPS cell lines): amplitude (two-tailed $t$-test, $P = 0.70$), threshold (two-tailed $t$-test, $P = 0.97$), rheobase (two-tailed Mann-Whitney test, $P = 0.22$), maximal rate of rise (two-tailed $t$-test, $P = 0.29$) and minimal rate of decay (two-tailed Mann-Whitney test, $P = 0.43$). Center shows median, box shows SEM and whisker represent 10th to 90th percentile. **d**, Representative traces from dissociated hCS neurons showing spontaneous action potentials (cell-attached mode) from control and 22q11DS neurons (control, $n = 3$ cells from 3 hiPS cell lines; 22q11DS, $n = 3$ cells from 3 hiPS cell lines).

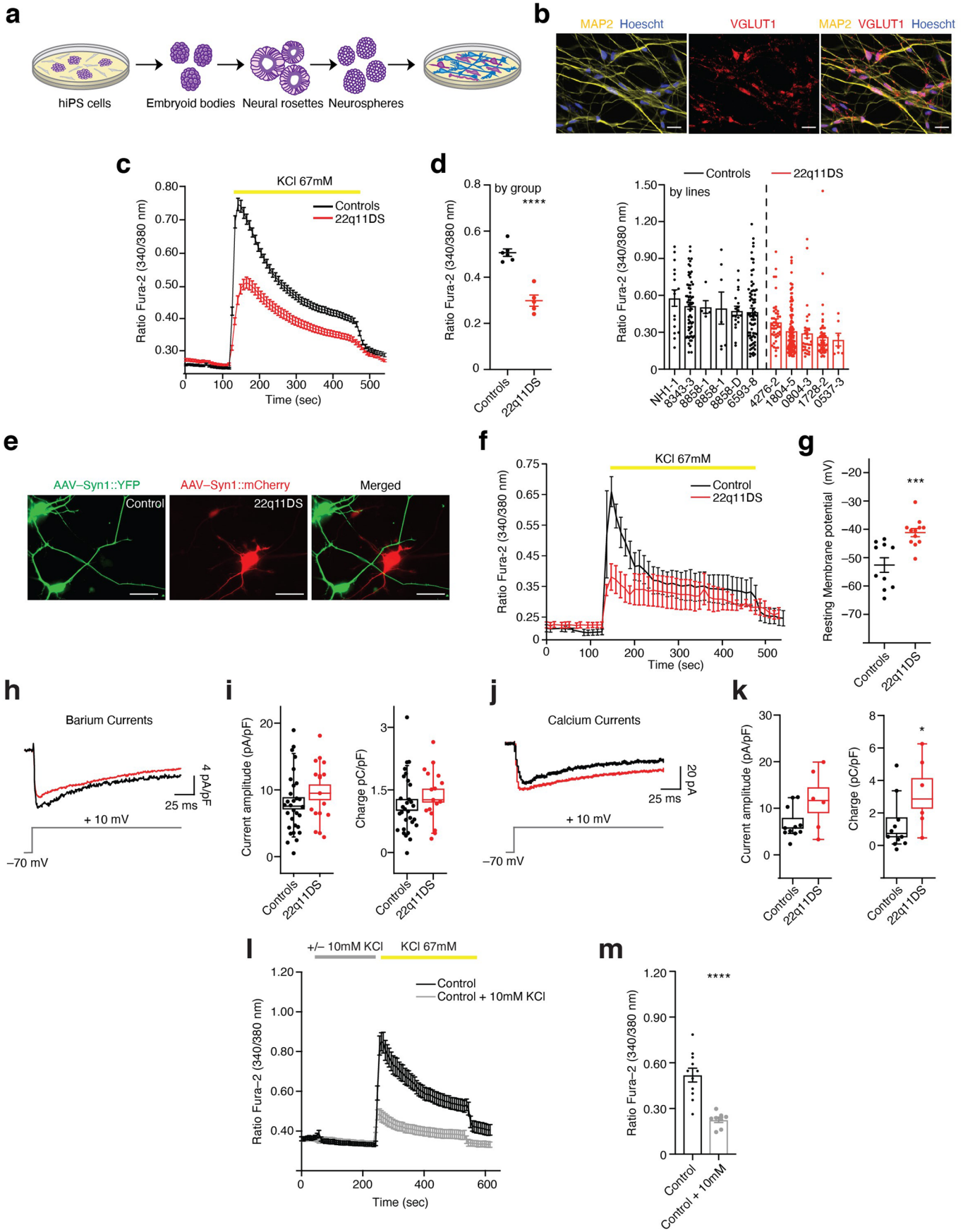


**Extended Data Fig. 6 | See next page for caption.**

**Extended Data Fig. 6 | Monolayer cortical differentiation and functional characterization of 22q11DS neurons. a**, Scheme illustrating the 2D-based approach for the differentiation of hiPS cells into cortical neural progenitor cells (NPCs) and cortical neurons. **b**, Immunostaining of neuronal cultures with anti-VGLUT1 and anti-MAP2 antibodies. Scale bar = 10µm. Representative images from one experiment. **c**, **d**, Changes in Fura-2 ratio in response to depolarization with 67 mM KCl (control, $n = 136$ cells from 6 lines derived from 4 subjects; 22q11DS, $n = 94$ cells from 5 lines derived from 5 subjects) and (d) quantification of Fura-2 ratio amplitudes shown by group and by hiPS cell (****$P < 0.0001$). Mean ratio ± SEM for (c). Mean peak amplitude ± SEM (d). **e**, Co-cultured 22q11DS and controls neurons with fluorescent labeling with AAV-DJ-hSyn1::mCherry or AAV-DJ-hSyn1::YFP. Images from over one experiment. **f**, Changes in Fura-2 ratio in response to depolarization with 67 mM KCl in co-cultured neurons (two-tailed Mann-Whitney for peak amplitude, $P < 0.0001$). Mean ratio ± SEM. Scale bar = 10µm **g**, RMP comparison (control, $n = 10$ neurons from one control line derived from 1 subject; 22q11DS, $n = 12$ neurons from 2 lines derived from 2 subjects. Mann-Whitney test, $P = 0.0005$). Mean ± SEM. **h**, Voltage dependent barium currents in 2D-derived neurons. Superimposed current traces before and during an activating step to 10 mV. **i**, Barium currents amplitude (left) and charge (right) (controls, $n = 30$ cells derived from 5 control hiPS cell lines derived from 5 subjects; 22q11DS, $n = 17$ cells derived from 4 patient hiPS cell lines derived from 4 subjects. Two-tailed Mann-Whitney, $P = 0.23$ for amplitude; two-tailed Mann-Whitney, $P = 0.28$ for charge). Center shows median, box shows SEM and whisker represent 10th to 90th percentile. **j**, Voltage dependent calcium currents in 2D-derived neurons. Superimposed current traces before and during an activating step to 10 mV. **k**, Calcium currents amplitude (left) and charge (right) (controls, $n = 11$ cells derived from 2 control hiPS cell lines derived from 2 subjects; 22q11DS, $n = 6$ cells derived from one patient hiPS cell lines derived from one subject. Two-tailed Mann-Whitney, $P = 0.17$ for amplitude; two-tailed Mann-Whitney, *$P = 0.04$ for charge). Center shows median, box shows SEM and whisker represent 10th to 90th percentile. **l**, The effect of 10 mM KCl pretreatment on Fura-2 calcium response to 67 mM KCl application in 2D derived control and 22q11DS neurons (control, $n = 11$ cells from one control hiPS cell line; control + 10mM, $n = 8$ from one control hiPS cell line). Mean ratio ± SEM. **m**, Quantification of the effect of 10 mM KCl pretreatment on the Fura-2 ratio amplitude from (l) (two-tailed Mann-Whitney for peak amplitude, ****$P < 0.0001$.) Mean peak amplitude ± SEM.

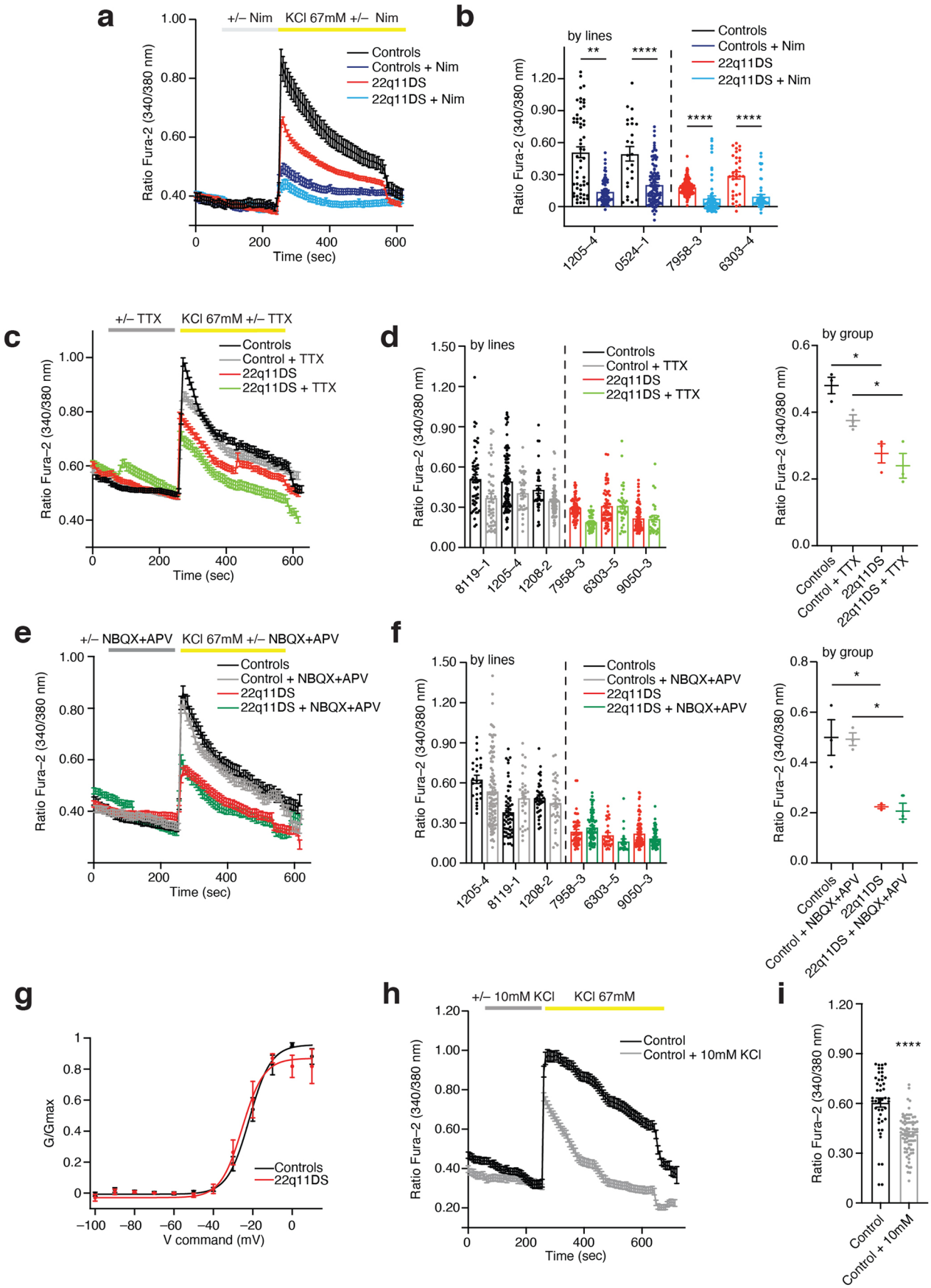


**Extended Data Fig. 7 | See next page for caption.**

**Extended Data Fig. 7 | Functional calcium signaling characterization of hCS-derived neurons in 22q11DS. a**, The effect of nimodipine (10 μM) on the calcium (Fura-2) response to 67 mM KCl application in control and 22q11DS neurons (control, $n = 68$ cells from 2 lines derived from 2 subjects; 22q11DS, $n = 192$ cells from 2 lines derived from 2 subjects; control + nimodipine, $n = 69$ cells from 2 lines derived from 2 subjects; 22q11DS+nimodipine, $n = 121$ cells from 2 lines derived from 2 subjects). Mean ratio ± SEM. **b**, Quantification of the effect of nimodipine on the Fura-2 ratio amplitude (Fura-2 ratio decreased by ~64% in control cortical and by ~57% in 22q11DS neurons; two-sided Kruskal–Wallis test, $P < 0.0001$; followed by Dunn's multiple comparison test; $^{**}P = 0.001$, $^{****}P < 0.0001$). Mean peak amplitude ± SEM. **c**, **d**, The effect of TTX (1 μM) on the Fura-2 calcium response following 67 mM KCl application in control and 22q11DS neurons (control: $n = 126$ cells from 3 hiPS cell line derived from 3 subjects; 22q11DS: $n = 230$ from 3 control hiPS cell line derived from 3 subjects; control + TTX: $n = 158$ cells from 3 hiPS cell line derived from 3 subjects; 22q11DS + TTX: $n = 107$ cells derived from 3 hiPS cell line derived from 3 subjects). (Right) Quantification of the effect of TTX on the Fura-2 ratio amplitude (two-way ANOVA for TTX exposure, $F_{1,8} = 6.50$, $^{*}P = 0.03$; Tukey's multiple comparison test: $^{**}P = 0.004$ for 22q11DS versus control, $^{*}P = 0.04$ for 22q11DS + TTX versus control + TTX). Mean ratio ± SEM for (c). Mean peak amplitude ± SEM for (d). **e**, **f**, The effect of APV (20 μM) and NBQX (20 μM) on the Fura-2 calcium response following 67 mM KCl application in control and 22q11DS neurons (control, $n = 120$ cells from 3 hiPS cell line derived from 3 subjects; 22q11DS, $n = 167$ from 3 control hiPS cell line derived from 3 subjects; control+NBQX+APV, $n = 167$ cells from 3 hiPS cell line derived from 3 subjects; 22q11DS + NBQX + APV, $n = 146$ cells derived from 3 hiPS cell line derived from 3 subjects). Peak amplitude ± SEM. (Right) Quantification of the effect of APV and NBQX on the Fura-2 ratio amplitude (two-way ANOVA for NBQX + APV exposure, $F_{1,8} = 0.08$, $P = 0.77$). Mean ratio ± SEM for (e). Mean peak amplitude ± SEM for (f). **g**, G/Gmax activation curve for calcium channels mediated currents, using 2 mM external barium as the main charge carrier (control, $n = 8$ cells from two hiPS cell lines; 22q11DS, $n = 7$ from two hiPS cell lines). Mean ± SEM. **h**, **i**, Effect of 10 mM KCl pretreatment on the Fura-2 calcium response after 67 mM KCl application in dissociated hCS control and 22q11DS neurons. (Right) Quantification of the effect of 10 mM KCl pretreatment on the Fura-2 ratio amplitude (control, $n = 44$ cells from one control hiPS cell line; control + 10mM, $n = 77$ from one control hiPS cell line derived; two-tailed Mann–Whitney for peak amplitude, $^{****}P < 0.0001$). Mean ± SEM. Mean ratio ± SEM for (h). Mean peak amplitude ± SEM for (i).

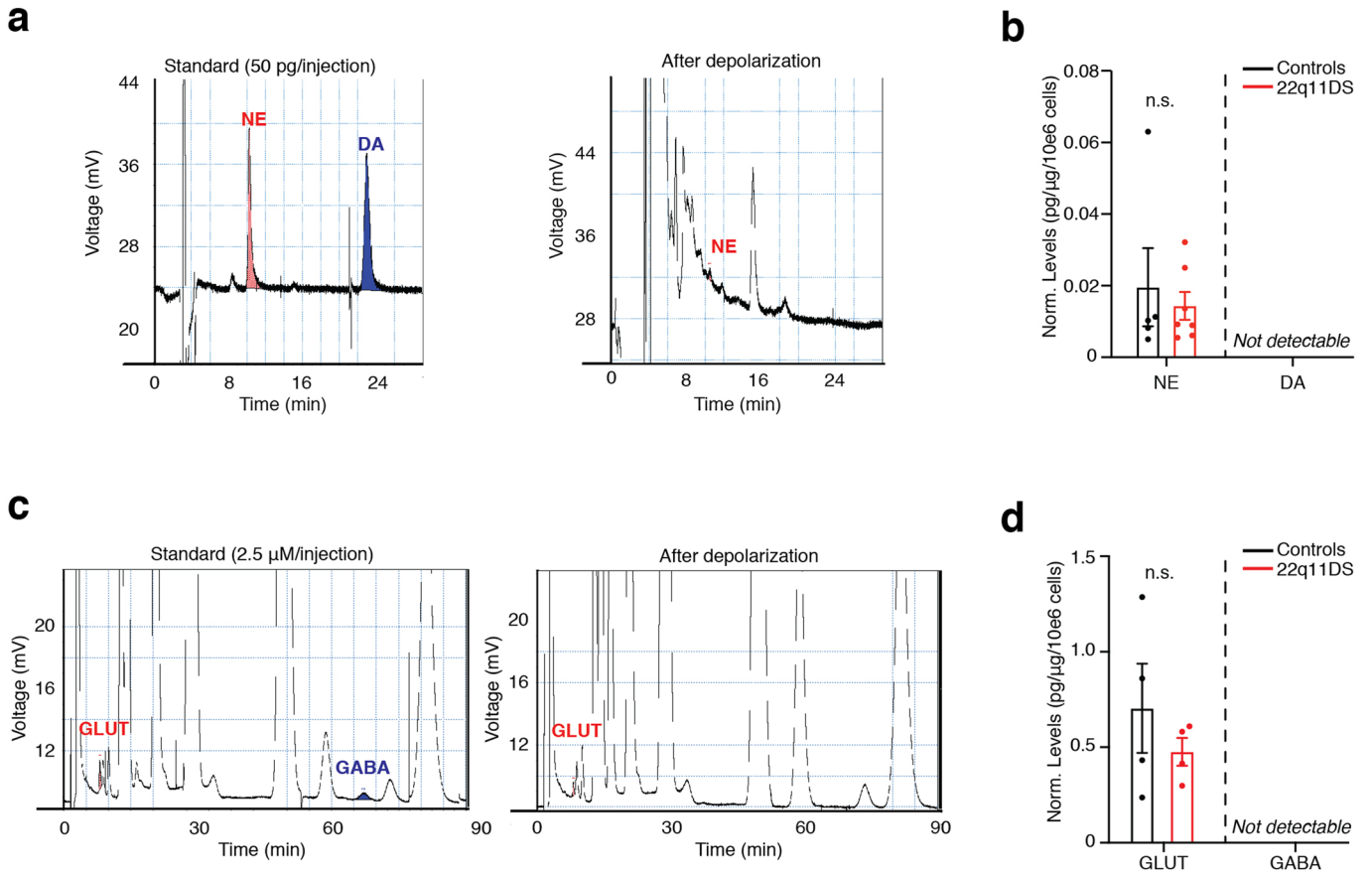


**Extended Data Fig. 8 | HPLC analysis of catecholamines, glutamate and GABA after depolarization of cortical neurons derived from control and 22q11DS patients. a**, and **c**, example chromatograms with the peaks for injected standard solutions of norepinephrine (NE), dopamine (DA), glutamate (GLUT), and GABA, and example of chromatograms in neuronal samples at day 43 of differentiation following depolarization with 67 mM KCl. **b**, and **d**, quantification of the levels of these neurotransmitters in control and 22q11DS media samples (results are normalized to the total number of cells). Two-sided *t*-test, $P = 0.72$ for NE, $P = 0.39$ for GLUT, DA and GABA not detectable (control: 4 hiPS cell lines derived from 3 subjects; 22q11DS, 5 hiPS cell lines derived from 5 subjects). Mean ± SEM.

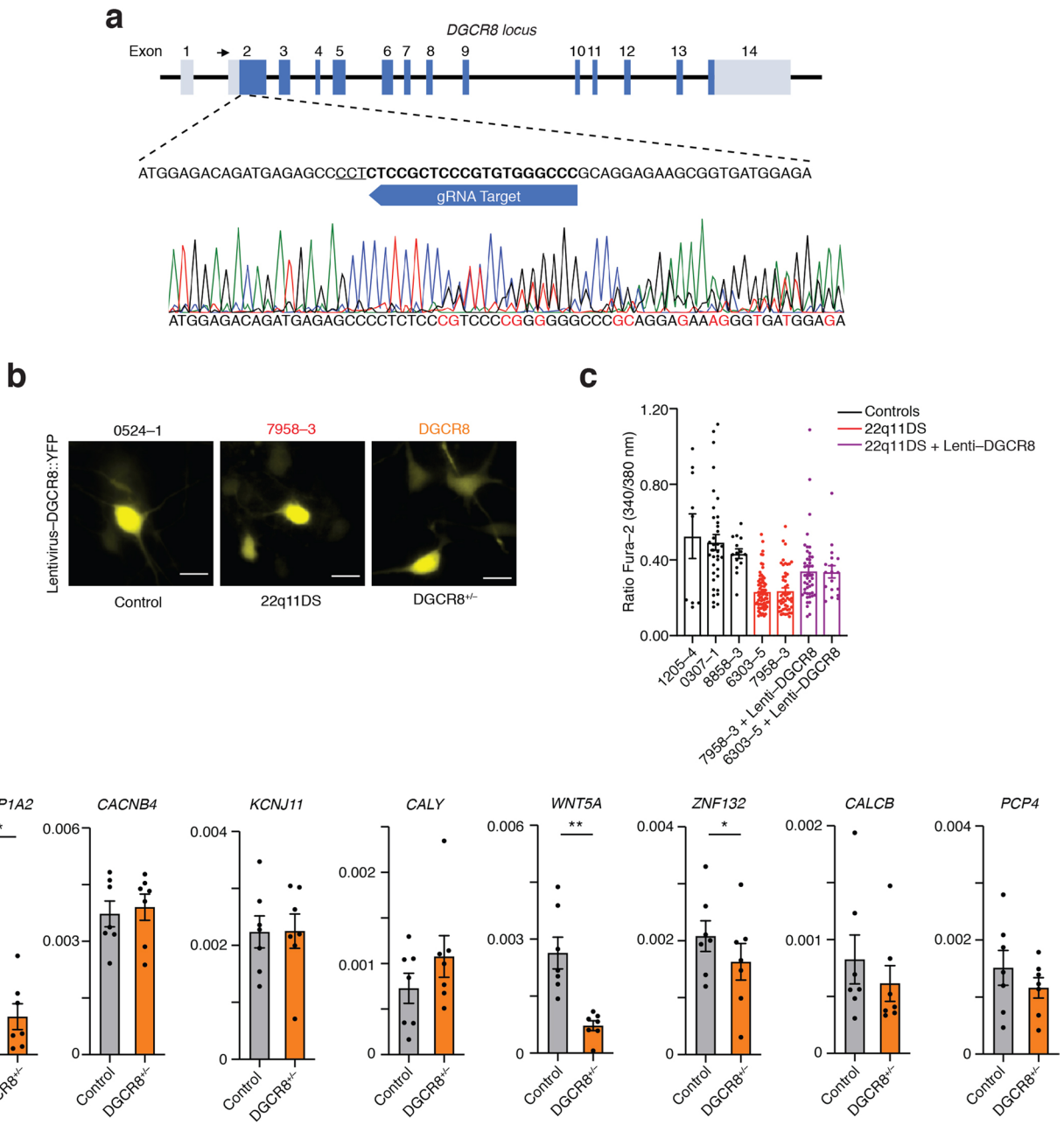


**Extended Data Fig. 9 | Generation and characterization of a DGCR8$^{+/-}$ hiPS cell line. a**, Scheme illustrating the CRISPR/Cas9 editing design of DGCR8 heterozygous knockout (DGCR8$^{+/-}$). **b**, Example images showing DGCR8 overexpression with the lentivirus-EF1α-DGCR8::YFP. Scale bar = 10 μm. Images from two experiments with similar results. **c**, Data from Fig. 5d shown by hiPS cell line. DGCR8 overexpression in control and 22q11DS dissociated hCS neurons (control, $n = 59$ cells from 3 hiPS cell lines derived from 3 subjects; 22q11DS, $n = 118$ cells from 2 hiPS cell lines derived from 2 subjects; 22q11DS + Lenti-DGCR8, $n = 64$ cells from two 22q11DS hiPS cell lines derived from 2 subjects). Mean peak amplitude ± SEM. **d**, Relative gene expression (normalized to *GAPDH*) as determined by RT-qPCR (day 75 of in vitro differentiation) in DGCR8$^{+/-}$ ($n = 7$ independent differentiation experiments of one DGCR8$^{+/-}$ hiPS cell line) versus isogenic control ($n = 7$ independent differentiation experiments of one parental hiPS cell line) of selected differentially expressed genes of 22q11DS RNA-seq from Supplementary Table 5: *ATP1A2* (two-tailed Wilcoxon test, $^{*}P = 0.02$), *WNT5A* (two-tailed Wilcoxon test, $^{**}P = 0.01$), and *ZNF132* (two-tailed Wilcoxon test, $^{*}P = 0.02$), *CACNB4* (two-tailed Wilcoxon test, $P = 0.94$), *KCNJ11* (two-tailed Wilcoxon test, $P = 0.94$), *CALY* (two-tailed Wilcoxon test, $P = 0.22$), *CALCB* (two-tailed Wilcoxon test, $P = 0.22$), *PCP4* (two-tailed Wilcoxon test, $P = 0.08$). Mean ± SEM.

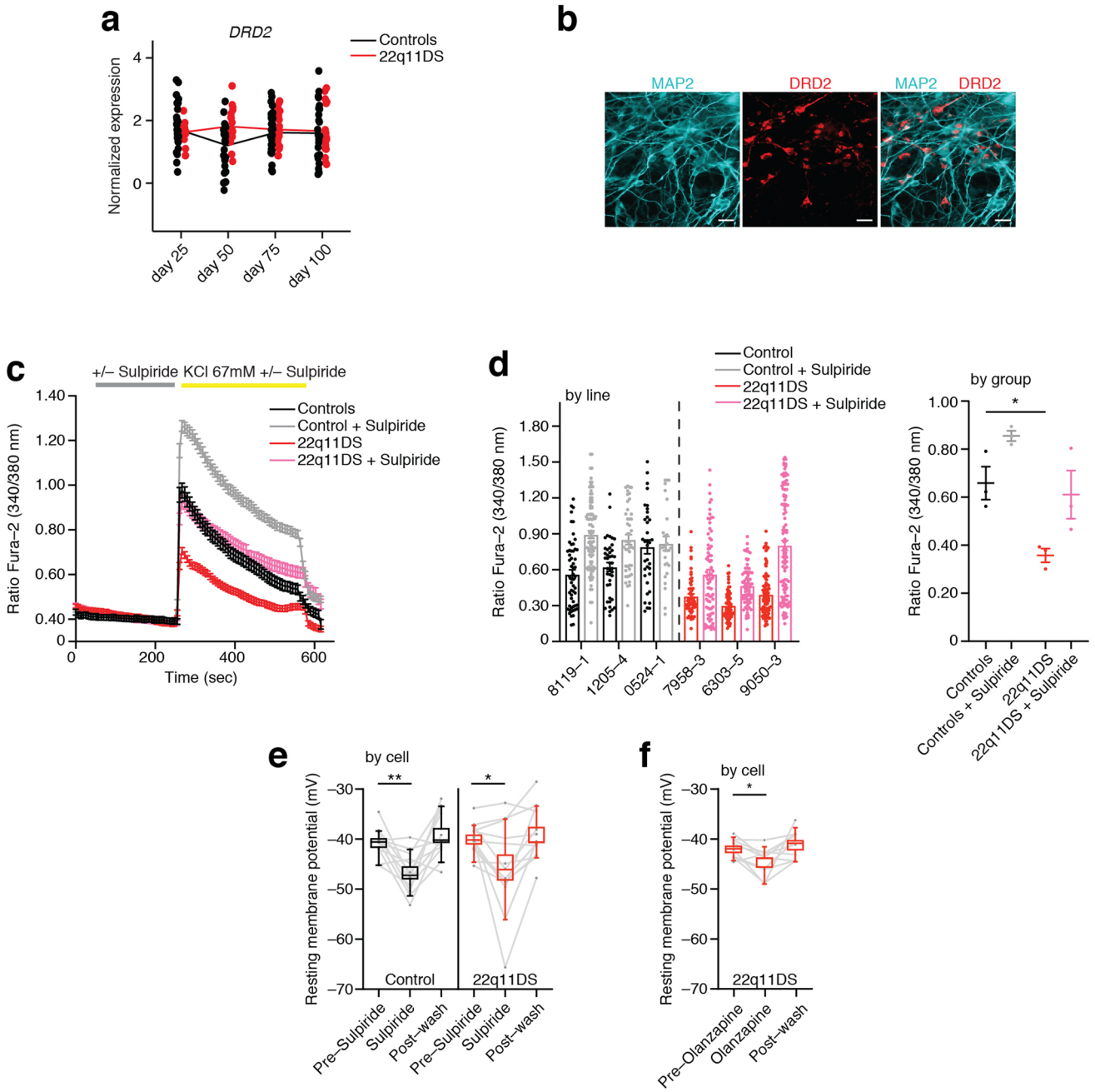


**Extended Data Fig. 10 | Pharmacological rescue with sulpiride and olanzapine. a**, Trajectory of *DRD2* gene expression (RNA-seq) in 22q11DS (red) and control lines (black) in hCS (controls, $n = 26$ (day 25 hCS), $n = 25$ (day 50 hCS), $n = 28$ (day 75 hCS), and $n = 25$ (day 100 hCS) samples from 14 control hiPS cell lines derived from 11 subjects; 22q11DS, $n = 14$ (day 25 hCS), $n = 16$ (day 50), $n = 24$ (day 75), and $n = 17$ (day 100) samples derived from 15 patient hiPS cell lines derived from 12 subjects). **b**, Immunostaining of hiPS cell-derived cortical neurons with anti-MAP2 and anti-DRD2 antibodies. Scale bar = 20 μm. Image from one experiment. **c**, Changes in Fura-2 ratio in response to 67 mM KCl in the presence or absence of 10 μM sulpiride. Mean ± SEM. **d**, Quantification of the peak Fura-2 ratio amplitude (control, $n = 133$ cells from 3 hiPS cell lines derived from 3 subjects; 22q11DS, $n = 215$ cells from 3 hiPS cell lines derived from 3 subjects; control + Sulpiride, $n = 166$ cells from 3 control hiPS cell lines derived from 3 subjects; 22q11DS + Sulpiride, $n = 253$ cells from 3 hiPS cell lines derived from 3 subjects; two-way ANOVA for sulpiride exposure, $F_{1,8} = 12.56$, $^{**}P = 0.008$; Tukey's multiple comparison test: $P = 0.95$ for 22q11DS + Sulpiride versus control, $P = 0.08$ for 22q11DS versus 22q11DS + Sulpiride; $P = 0.20$ for control versus control + Sulpiride; $^{*}P = 0.04$ for 22q11DS versus control). Mean peak amplitude ± SEM. **e**, The effect of sulpiride on the membrane potential of control and 22q11DS neurons ($n = 12$ control neurons, one-way repeated measures ANOVA, $F_{2,22} = 14.35$, $^{****}P < 0.0001$; followed by Tukey's multiple comparisons test: $^{**}P = 0.001$ for pre-sulpiride versus sulpiride, $^{****}P < 0.0001$ for sulpiride versus post-wash, $P = 0.56$ for pre-sulpiride versus post-wash; $n = 13$ 22q11DS neurons, one-way repeated measures ANOVA, $F_{2,22} = 7.84$, $^{*}P = 0.002$; Tukey's multiple comparisons test: $^{*}P = 0.01$ for pre-sulpiride versus sulpiride, $^{**}P = 0.003$ for sulpiride versus post-wash and $P = 0.72$ for pre-sulpiride versus post-wash). Center shows median, box shows SEM and whisker represent 10th to 90th percentile. **f**, The effect of olanzapine on the RMP of 22q11DS neurons ($n = 10$ neurons derived from one 22q11DS hiPS cell line, one-way repeated measures ANOVA, $F_{2,18} = 6.3$, $^{**}P = 0.008$; followed by Tukey's multiple comparisons test: $^{*}P = 0.05$ for pre-olanzapine versus olanzapine, $^{**}P = 0.008$ for olanzapine versus post-wash, $P = 0.69$ for pre-olanzapine versus post-wash). Center shows median, box shows SEM and whisker represent 10th to 90th percentile.

nature research

Corresponding author(s): Sergiu P. Pasca

Last updated by author(s): July 10, 2020

# Reporting Summary

Nature Research wishes to improve the reproducibility of the work that we publish. This form provides structure for consistency and transparency in reporting. For further information on Nature Research policies, see Authors & Referees and the Editorial Policy Checklist.

## Statistics

For all statistical analyses, confirm that the following items are present in the figure legend, table legend, main text, or Methods section.

| n/a | Confirmed | |
|---|---|---|
| ☐ | ☒ | The exact sample size (*n*) for each experimental group/condition, given as a discrete number and unit of measurement |
| ☐ | ☒ | A statement on whether measurements were taken from distinct samples or whether the same sample was measured repeatedly |
| ☐ | ☒ | The statistical test(s) used AND whether they are one- or two-sided<br>*Only common tests should be described solely by name; describe more complex techniques in the Methods section.* |
| ☐ | ☒ | A description of all covariates tested |
| ☐ | ☒ | A description of any assumptions or corrections, such as tests of normality and adjustment for multiple comparisons |
| ☐ | ☒ | A full description of the statistical parameters including central tendency (e.g. means) or other basic estimates (e.g. regression coefficient) AND variation (e.g. standard deviation) or associated estimates of uncertainty (e.g. confidence intervals) |
| ☐ | ☒ | For null hypothesis testing, the test statistic (e.g. *F*, *t*, *r*) with confidence intervals, effect sizes, degrees of freedom and *P* value noted<br>*Give P values as exact values whenever suitable.* |
| ☒ | ☐ | For Bayesian analysis, information on the choice of priors and Markov chain Monte Carlo settings |
| ☒ | ☐ | For hierarchical and complex designs, identification of the appropriate level for tests and full reporting of outcomes |
| ☐ | ☒ | Estimates of effect sizes (e.g. Cohen's *d*, Pearson's *r*), indicating how they were calculated |

*Our web collection on statistics for biologists contains articles on many of the points above.*

## Software and code

Policy information about availability of computer code

| | |
|---|---|
| Data collection | Data collection: 10x Genomics Chromium Single Cell 3' chip, Igor Pro (Wavemetrics), pCLAMP 10.6 (Molecular Devices), OCULAR (Qimaging), Eclipse TE2000U (Nikon), Openlab software (PerkinElmer), Leica TCS SP8 confocal, Hiseq400. |
| Data analysis | RNA-bulk sequencing: tidyverse v1.2.10, fgsea 1.10.1, nlme v3.1.143, multcomp v1.4.12, variancePartition v1.14.1, PROPER v1.10.0, LDscore v1.0.0, picard tools v2.5.0, STAR v2.5.2b, rsem v1.3.0, GATK v3.3, plink v1.08, HapMap3.3 (hg38).<br><br>Single-cell RNA-seq:10x Genomics Chromium Single Cell 3' GEM, Library & Gel Bead Kit v2, NovaSeq S4 Data analysis: Cell Ranger v3.0, R version 3.6.1, Seurat v3.0, ggplot2 v3.2.1, pheatmap v1.0.12.<br><br>Graphing and statistical analysis: GraphPad Prism v8, Igor Pro (Wavemetrics), MATLAB (Simulink), pCLAMP 10.6 (Molecular Devices), Image J (FIJI), OriginPro 2016 (OriginLab), JMP v15 (SAS).<br><br>RT-qPCR: QuantStudio RT–qPCR software (v1.1, Applied Biosystems).<br><br>Only existing software tools were used for this study. |

For manuscripts utilizing custom algorithms or software that are central to the research but not yet described in published literature, software must be made available to editors/reviewers. We strongly encourage code deposition in a community repository (e.g. GitHub). See the Nature Research guidelines for submitting code & software for further information.

## Data

Policy information about availability of data

All manuscripts must include a data availability statement. This statement should provide the following information, where applicable:

- Accession codes, unique identifiers, or web links for publicly available datasets
- A list of figures that have associated raw data
- A description of any restrictions on data availability

Bulk RNA-seq: GSE142041
Single-cell RNA-seq: GSE145122
BrainSpan (dbGaP Study Accession: phs000755.v2.p1), HapMap3.3 (hg38) (https://www.sanger.ac.uk/resources/downloads/human/hapmap3.html)

# Field-specific reporting

Please select the one below that is the best fit for your research. If you are not sure, read the appropriate sections before making your selection.

☒ Life sciences ☐ Behavioural & social sciences ☐ Ecological, evolutionary & environmental sciences

For a reference copy of the document with all sections, see nature.com/documents/nr-reporting-summary-flat.pdf

# Life sciences study design

All studies must disclose on these points even when the disclosure is negative.

| | |
|---|---|
| Sample size | Sample sizes were estimated based on previous studies in the field. Power analysis conducted for RNA-seq. |
| Data exclusions | hiPS cell lines with high number of duplication and deletions were excluded from experiments and analysis. |
| Replication | Experiments were performed from hiPS cells derived from 15 subjects with 22q11DS and 15 control subjects. For assay, we examined hCS and 2D neurons from multiple differentiation experiments. Replicates for each type of experiment are indicated in the manuscript and in the Supplementary Table 2. |
| Randomization | hCS of similar diameter were randomly selected for gene expression experiments. Neurons for patching and imaging were randomly selected using cell-specific fluorescent reporters. All other samples were randomly collected and allocated into their respective groups. |
| Blinding | The investigators were blinded to the genetic background (control, 22q11DS and DGCR8+/-) for all patch clamping experiments. Experiments in the large scale calcium phenotyping assay in Fig 2d were conducted blind to disease status. |

# Reporting for specific materials, systems and methods

We require information from authors about some types of materials, experimental systems and methods used in many studies. Here, indicate whether each material, system or method listed is relevant to your study. If you are not sure if a list item applies to your research, read the appropriate section before selecting a response.

### Materials & experimental systems

| n/a | Involved in the study |
|---|---|
| ☐ | ☒ Antibodies |
| ☐ | ☒ Eukaryotic cell lines |
| ☒ | ☐ Palaeontology |
| ☒ | ☐ Animals and other organisms |
| ☐ | ☒ Human research participants |
| ☒ | ☐ Clinical data |

### Methods

| n/a | Involved in the study |
|---|---|
| ☒ | ☐ ChIP-seq |
| ☒ | ☐ Flow cytometry |
| ☒ | ☐ MRI-based neuroimaging |

## Antibodies

| | |
|---|---|
| Antibodies used | Rat anti-CTIP2 (Abcam, AB18465), used 1:300<br>Guinea Pig anti-MAP2 (Synaptic Systems, 188044), used 1:5000<br>Rabbit anti–DRD2 (Frontier Institute, D2R–Rb–Af960; previously cataloged as Frontier Institute, D2R–Rb–Af750), used 1:300<br>Rabbit anti-VGLUT1 (Synaptic Systems, 135302), used 1:500<br>StemLight Pluripotency Antibody Kit (Cell Signaling Technology, 9656S) was used for OCT4, NANOG, SSEA–3, TRA–1–60, TRA–2–49, used 1:200 dilution for all antibodies in the kit. |
| Validation | Some of the antibodies (MAP2, CTIP2) were validated in our previous studies (Pasca, Sloan et al., Nature Methods 2015; Sloan et al., Neuron, 2017; Birey, Andersen, Makinson et al., Nature, 2017; Sloan, Andersen, Pasca, Birey et al., Nature Protocols, 2018). |

The rat anti-CTIP2 (Abcam, AB18465) has been used in 240 studies according manufacturer's website, and tested for immunofluorescence staining in human fetal brains (Ozai et al., 2018).
The rat anti-MAP2 (Synaptic Systems, 188044) has been used in 54 studies according to manufacturer's website.
The rabbit anti-DRD2 (Frontier Institute, D2R–Rb–Af960; previously Frontier Institute, D2R–Rb–Af750) has been used in multiple studies according to manufacturer's website.
The Rabbit anti-VGLUT1 (Synaptic Systems, 135302) has been used in 27 ICC and 30 IHC studies according to manufacturer's website.
StemLight Pluripotency Antibody Kit (Cell Signaling Technology, 9656S, 1:200 dilution for all antibodies in kit) was used for OCT4, NANOG, SSEA–3, TRA–1–60, TRA–2–49 and has been cited in 3 other studies according to manufacturer's website.

## Eukaryotic cell lines

Policy information about cell lines

| | |
|---|---|
| Cell line source(s) | The hiPS cell lines were derived at Stanford University with IRB approval and under informed consent. Some of the fibroblasts for cell reprogramming were obtained at NIMH.<br>Inactivated mouse fibroblasts EmbryoMax PMEF fro hiPS cell culture were purchased from EMD Millipore. |
| Authentication | All hiPS cell lines were assessed for genomic integrity by SNP microarray "GSAMD–24v2–0" (with 759,993 probes).<br>Most hiPS cell lines were assessed for pluripotency (Pasca et al, Nature Medicine 2011 or Yazawa et al., Nature 2011) |
| Mycoplasma contamination | All cell lines and PMEF were regularly tested for Mycoplasma contamination and tested negative. |
| Commonly misidentified lines<br>(See ICLAC register) | No commonly misidentified cell lines were used |

## Human research participants

Policy information about studies involving human research participants

| | |
|---|---|
| Population characteristics | 15 patients with 22q11DS (22.8 ± 2.4 years; female to male ratio: 60% to 40%) and 15 controls (23.8 ± 4.0 years; female to male ratio: 67% to 33%. Detailed clinical data provided in Supplementary Table 1. |
| Recruitment | Subjects were recruited at Stanford University, UCLA, NIMH. |
| Ethics oversight | Stanford University, UCLA, NIMH. |

Note that full information on the approval of the study protocol must also be provided in the manuscript.